photonics

MDPI

Article

Partially Coherent Imaging in Dark-Field and Differential Phase-Contrast Microscopy

Colin J. R. Sheppard *, Alan P. Blood and Maitreyee Roy

School of Optometry and Vision Science, Faculty of Medicine and Health, University of New South Wales (UNSW Sydney), Sydney, NSW 2052, Australia; alan.blood@unsw.edu.au (A.P.B.); maitreyee.roy@unsw.edu.au (M.R.)
* Correspondence: colinjrsheppard@gmail.com

Abstract

The theory of partially coherent image formation in dark-field and phase-contrast microscopy is presented. Explicit expressions and three-dimensional plots of the transmission cross-coefficient for different imaging modes are given. These include central and oblique internal dark field, annular dark field, phase contrast, differential phase contrast using semicircular or quadrant condenser pupils, and differential interference contrast. Explicit expressions are given for the image intensity for pure-phase objects consisting of a single-object spatial frequency or combinations of object frequencies.

Keywords: imaging; microscopy; dark field; phase contrast; partial coherence

1. Introduction

In a recent paper, we reviewed visual observation methods for dark-field and phase-contrast microscopy [1]. Although recently, there have been many developments aimed at quantitative imaging, especially of phase, using computational techniques, visual observation is still important and widely used, for example, in pathology. Our paper specifically includes internal dark-field imaging, a coherent imaging technique using plane-wave illumination at an oblique angle within the pupil of the objective lens, with a stop in a Fourier plane. However, in general, dark-field and phase-contrast techniques are partially coherent in nature. In the present paper, we attempt to introduce the theoretical background of partially coherent image formation in an understandable way. We consider a variety of systems, including dark field, phase contrast, differential phase contrast (DPC), and differential interference contrast (DIC), and give a unified comparison of the transmission cross-coefficients (TCCs) for various different systems. For DPC, we include semicircular and quadrant condenser pupils, as well as a first-moment pupil.

Although other methods for image modelling may be preferable for an object consisting of a point, two points or a line, the TCC method is particularly useful for modelling grating structures. Explicit expressions are given for partially coherent images of a pure-phase object consisting of a single spatial frequency. As some systems give rise to images only of higher harmonics of the object frequency, we also consider objects with two object frequencies, resulting in sum and difference frequencies.

Most methods of quantitative phase imaging in partially coherent systems are based on the assumption of either a weakly scattering or a slowly varying object. A weakly scattering theory (in the present sense) not only neglects multiple scattering but also neglects interference of scattered light with scattered light. A slowly varying theory cannot cover objects with variations near the resolution limit. On the other hand, a full partially

Check for updates

Received: 25 March 2026
Revised: 24 April 2026
Accepted: 18 May 2026
Published: 24 May 2026

Copyright: © 2026 by the authors. Licensee MDPI, Basel, Switzerland. This article is an open access article distributed under the terms and conditions of the Creative Commons Attribution (CC BY) license.

coherent theory does not have these limitations, although it is still based on a non-rigorous theory for the interaction with the sample. It can be used for forward calculation of images, but we do not attempt the inverse problem, although it could be developed for objects that exhibit a combination of both weak (high frequency) and slowly varying components.

2. Partially Coherent Image Formation

It is interesting to recall that Abbe's theory of resolution was based on the assumption of coherent illumination [2] and, as a result, was criticised because practical microscope systems use an extended source [3]. Although this limitation was, to some extent, resolved by Rayleigh's analysis [4,5], it was not until Hopkins' paper in 1953 that the full theory of partially coherent imaging was introduced [6].

There are basically three ways to calculate partially coherent images. The first is by direct integration over the intensity of the coherent images produced by plane-wave illumination from individual points on the incoherent condenser [4]. The second way involves the introduction of the transmission cross-coefficient (TCC), a bilinear transfer function [6]. This paper is mainly concerned with this approach. An advantage is that calculation of the TCC only involves source distributions and pupil functions rather than specifically involving partial coherence theory as such. Once the TCC has been specified, images of a variety of objects can then be calculated. The third way involves coherent mode decomposition, where the modes are a set of orthogonal modes [7,8]. There have been surprisingly few papers that have been devoted to partially coherent imaging in optical microscopy. A few more exist for electron microscopy [9,10]. Areas that have seen more extensive treatment include optical lithography [8], microdensitometry [11], dimensional metrology [12], and optical signal processing [13], perhaps partly because researchers in these areas are more likely to have a physics background.

In this paper, we restrict our treatment to a scalar, paraxial, in-focus theory, where the light transmitted by a thin object is given by the product of the illuminating field and the object-amplitude transmittance. A coherent imaging system is linear in amplitude, so the aperture stop of the objective acts as a low-pass filter. The amplitude transmission is $t(\mathbf{v})$, where $\mathbf{v} = (x, y)$ is a normalised distance vector ($\mathbf{v} = 2\pi\mathbf{x}(NA)/\lambda$, with NA representing the numerical aperture ($n \sin \alpha$), α representing the angle of semi-convergence of the objective and n corresponding to the refractive index of immersion). The spatial frequency content of the object $T(\mathbf{m})$, where $\mathbf{m} = (m_x, m_y)$ is a normalised spatial frequency vector; thus, the Fourier transform of the amplitude transmission is filtered by a coherent transfer function ($c(\mathbf{m})$). For a plain, circular pupil, the filter has a constant magnitude within the aperture and drops to zero at the edge of the aperture stop when the magnitude of the normalised spatial frequency is $m = 1$. This corresponds to a true spatial frequency cut-off of NA/λ. The image amplitude is then given by the Fourier transform of the filtered amplitude, and its intensity is given by the squared magnitude of the Fourier transform. This is basically the theory presented by Abbe [2]. It is interesting to note that the Fourier transform (of a Fourier transform) gives an inverted image, but the inverse Fourier transform gives the image in the correct orientation, yielding the following for the image intensity:

$$\begin{aligned} I(\mathbf{v}) &= \left| \int c(\mathbf{m}) T(\mathbf{m}) \exp(i\mathbf{m}.\mathbf{v}) \, \mathrm{d}\mathbf{m} \right|^2 \\ &= \iint c(\mathbf{m}_1) c^*(\mathbf{m}_2) T(\mathbf{m}_1) T^*(\mathbf{m}_2) \exp[i(\mathbf{m}_1 - \mathbf{m}_2).\mathbf{v}] \, \mathrm{d}\mathbf{m}_1 \mathrm{d}\mathbf{m}_2. \end{aligned} \quad (1)$$

Thus, the corresponding spatial frequency in the intensity image is the difference frequency, i.e., $\mathbf{m}_1 - \mathbf{m}_2 = \mathbf{m}'$. The maximum spatial frequency in the image is $m'_{\max} = 2$ when $m_1 = 1$ and $m_2 = -1$. We can also introduce the central frequency, i.e., $\mathbf{m} = \frac{1}{2}(\mathbf{m}_1 + \mathbf{m}_2)$, so that

$\mathbf{m}_1 = (\mathbf{m} + \mathbf{m}'/2)$, $\mathbf{m}_2 = (\mathbf{m} - \mathbf{m}'/2)$. The $\mathbf{m}, \mathbf{m}'$ coordinates constitute an orthonormal system, with $\mathrm{d}\mathbf{m}_1\mathrm{d}\mathbf{m}_2 = \mathrm{d}\mathbf{m}\mathrm{d}\mathbf{m}'$ as the Jacobian of the transformation, equal to unity. We call $T(\mathbf{m}_1)T^*(\mathbf{m}_2)$ the object bilinear spectrum and $T(\mathbf{m} + \mathbf{m}'/2)T^*(\mathbf{m} - \mathbf{m}'/2) = M_T(\mathbf{m}; \mathbf{m}')$ the object mutual spectrum [14]. An analogous procedure can be applied to real space so that the central and difference coordinates are $\mathbf{v} = \frac{1}{2}(\mathbf{v}_1 + \mathbf{v}_2)$ and $\mathbf{v}' = \mathbf{v}_1 - \mathbf{v}_2$.

For a partially coherent system, Equation (1) still holds, but the product $(c(\mathbf{m}_1)c^*(\mathbf{m}_2))$ no longer separates and is replaced by the TCC, i.e., $C(\mathbf{m}_1; \mathbf{m}_2)$. Partially coherent imaging can therefore be regarded as a generalisation of coherent imaging of intensities. Imaging of a general object is based on the bilinear TCC, which is a function of pairs of spatial frequencies [6]. For a microscope with an infinite, uniform, incoherent source and either Köhler or critical illumination with a condenser pupil ($P_C(\mathbf{m})$) and objective pupil ($P_O(\mathbf{m})$), the TCC is given by

$$C(\mathbf{m}_1; \mathbf{m}_2) = \int |P_C(\boldsymbol{\xi})|^2 P_O(\boldsymbol{\xi} - \mathbf{m}_1) P_O^*(\boldsymbol{\xi} - \mathbf{m}_2) \mathrm{d}\boldsymbol{\xi}. \tag{2}$$

As intensity is a real quantity, $C(\mathbf{m}_1; \mathbf{m}_2) = C^*(\mathbf{m}_2; \mathbf{m}_1)$. We can write $C(\mathbf{m}_1; \mathbf{m}_2) = C'(\mathbf{m}; \mathbf{m}')$, where C' is basically a rotated and scaled version of the TCC. Note that $\mathbf{m}_1, \mathbf{m}_2$ are spatial frequencies in the same ($\mathbf{x}$) direction, even though they are often plotted orthogonally. We call C' the phase-space imager window (PSI window) [15]. Then, $C'(\mathbf{m}; \mathbf{m}') = C'^*(\mathbf{m}; -\mathbf{m}')$.

Hopkins and Barham pointed out (in 1950) that, "It is unfortunate that critical and Köhler illumination are designated in French by the terms 'éclairage incohérente' and 'éclairage cohérente' respectively", signifying how misunderstood partially coherent imaging was at that time [16].

This model assumes that the field of view is infinite. $|P_C(\boldsymbol{\xi})|^2 = S(\boldsymbol{\xi})$ is called the effective source. The ratio of $S = NA_C/NA_O$, called the coherence ratio, controls the coherence of the imaging process, which determines the resolution. For $S = 0$, the system reduces to coherent imaging (linear in complex amplitude), while for $S \to \infty$, it becomes incoherent (linear in intensity). As S increases, in general, resolution increases and contrast decreases. In practice, $S \approx 0.75$ gives a compromise. $S = 1$ is called full, matched, or complete illumination. Some papers have incorrectly stated that $S = 1$ gives incoherent imaging, although the images are similar but not identical. The Rayleigh two-point resolution is identical for $S = 1$ and $S \to \infty$, but the intensities at the edge position for a unit-step object occur at 1/3 and 1/2. Low values of S (e.g., ≈0.25) are often used in metrological applications, as then, the gradient of the intensity at an edge is large, increasing measurement sensitivity.

Partially coherent imaging theory is unfortunately complicated, so it is useful to consider simplified, approximate cases. For a weakly scattering object such that interference of scattered light with scattered light can be neglected, the image is determined by the weak object transfer function (WOTF), i.e., $C(\mathbf{m}_1; \mathbf{0}) = C^*(\mathbf{0}; \mathbf{m}_2)$, so that difference (or sum) frequencies are no longer present in the image. Most of the early literature on phase contrast was based on the assumption of weak scattering [17]. Note that for a strong grating consisting of even a single sinusoidal spatial-frequency (m_0) variation in thickness, there are frequency components imaged by $C(\pm m_0, \pm m_0)$ that produce a constant intensity in the image ($m' = 0$), as well as components $C(\pm m_0, \mp m_0)$, which produce second-harmonic (frequency-doubled) intensity variations in the image with $m' = \pm 2m_0$.

The WOTF does not provide a complete description for imaging of a general object. In particular, an object with a constant phase gradient ($\mathrm{d}\phi/\mathrm{d}x$), with an object function of $t(\mathbf{x}) = a \exp i\phi = a \exp(i\mathbf{m}_0.\mathbf{v}_\mathbf{x})$, contains only a single spatial frequency, i.e., $\mathbf{m}_1 = \mathbf{m}_2 = \mathbf{m}_0$, so that the image intensity is $I = a^2 C(\mathbf{m}_0; \mathbf{m}_0)$. Examples of such objects include a sloping surface in reflection, a small-angled prism, and a refractive index

differing from the bulk in transmission. The prism deflects the illuminating beam so that it is displaced relative to the objective pupil. As $\mathbf{m}' = \mathbf{0}$, $C(\mathbf{m};\mathbf{m}) = C'(\mathbf{m};\mathbf{0})$, and the spatial frequency in the image is zero. However, if the phase gradient is slowly varying compared with the point-spread function of the system, then $\mathbf{m}_0(\mathbf{v_x})$ is a slowly varying function of $\mathbf{v_x}$, and the image intensity is also slowly varying. $C(\mathbf{m};\mathbf{m})$ is called the phase-gradient transfer function (PGTF), although it is not strictly a transfer function but a section through the TCC.

The PGTF also does not provide a complete description of imaging, which is given by filtering the object bilinear spectrum through the PSI-window, then integrating m and inverse Fourier transformation in $\mathbf{m}'$ [15]. This approach is particularly appropriate for calculation of images of periodic grating structures, as the object is then described simply as a series of delta functions in Fourier space.

Some simple objects can be calculated more simply in real space than using the TCC. The image of a single bright point is found to be independent of S, as there is only a single point to be illuminated. However, interestingly, this is not the case for Nomarski DIC, when the point-spread function (PSF) does depend on the value of S [18]. The equivalent of the PSF for partially coherent imaging, called the phase-space imager kernel (PSI-kernel), is given by the Fourier transform of the PSI-window in $\mathbf{m}'$.

The Rayleigh two-point resolution criterion does depend on the value of S [16]. The resolution improves as S is increased from the coherent case, reaches an optimum at $S \approx 1.45$, then oscillates such that resolution is identical for $S = 1$ and $S \to \infty$. Two-point resolution was shown by McKechnie to be improved by using an annular condenser [19].

Images of an opaque edge for different values of S were presented by Watrasiewicz and by Kinzly [20,21]. The coherent image exhibits strong fringing, which decreases as S increases. However, the intensity gradient at the edge increases as S decreases, thereby improving the sensitivity of edge detection. The intensity at the edge, itself, changes with S, being half of the maximum value for the incoherent case ($S \to \infty$), $1/4$ for the coherent case ($S = 0$), and $1/3$ for the matched case ($S = 1$), which is an important consideration for the sizing of objects.

3. More General Systems

Hopkins' theory is based on the assumption of an infinite, incoherent source. If the source is finite and fully coherent and critical illumination is employed, the system images not the object itself but the illuminated object, thereby limiting the field of view [22,23]. If the source is partially coherent, the behaviour is even more complicated.

Another important case is that of a scanning microscope system. If the collection system measures the intensity of the light from the object, according to the reciprocity theorem, the system gives the same image as a conventional microscope, but now, S is given by the ratio of the numerical aperture of the collector to that of the objective lens used as a scan lens, i.e., $S = NA_{Coll}/NA_O$ [24]. The collection system can be arranged to be either critical or Köhler detection, in analogy with the illumination system of a conventional microscope [25]. If, on the other hand, the collector lens focuses light onto a point detector, the system becomes a confocal microscope [25]. A confocal (non-fluorescence) microscope behaves as a coherent imaging system, with a point-spread function given by the product of those for the objective and collector lenses and a CTF given by the convolution of the CTFs of the two lenses. More general systems have partially coherent sources and/or finite-sized detector pinholes [26,27].

4. Partially Coherent System with Aberration-Free Circular Pupils

For two plain, circular pupils ($S = 1$), the TCC is given by the area of overlap of three mutually displaced circles: the effective source ($|P_C|^2$), the objective pupil (P_O) and its complex conjugate (P_O^*). For two equal circles, for line structures (such that $m_{1y} = m_{2y} = 0$), the TCC in the x direction is given by

$$\begin{aligned} C(m_1;m_2) =& \Lambda(|m_1|), && |m_1| \geq |m_2|, \operatorname{sgn} m_2 = \operatorname{sgn} m_1 \\ =& \Lambda(|m_2|), && |m_2| \geq |m_1|, \operatorname{sgn} m_2 = \operatorname{sgn} m_1 \\ =& \Lambda(|m_1 - m_2|), && \operatorname{sgn} m_2 = -\operatorname{sgn} m_1, \end{aligned} \tag{3}$$

where Λ for positive m is the normalised convolution of two circles (area of overlap of two mutually displaced circles), i.e.,

$$\begin{aligned} \Lambda(m) =& \frac{2}{\pi}\left[\arccos\left(\frac{m}{2}\right) - \frac{m}{2}\sqrt{1-\left(\frac{m}{2}\right)^2}\right], && m \leq 2 \\ =& 0, && m \geq 2, \end{aligned} \tag{4}$$

which is also the optical transfer function (OTF) for incoherent imaging by a circular pupil. Note that our expression for the Λ function here is also defined for a negative m, which can sometimes be useful when it is different from the OTF. For a negative m, the OTF is $\Lambda(|m|) = 2 - \Lambda(m)$.

The TCC for a system with two equal plain, circular pupils is shown as a 3D plot in Figure 1a. A similar 3D plot was sketched in Reference [25]. Analytical expressions for different values of S were given by Kintner [28]. Contour plots for different values of S and including the effects of defocus and spherical aberration were presented by Möller [29].

We find that the WOTF ($C(m;0)$) and the PGTF ($C(m;m)$) are equal to each other, and both are equal to $\Lambda(|m|)$ so that both cut off at $m = 2$. These results can be generalised for $0 \leq S \leq 1$, with cut-offs of $(1 + S)$, indicating that resolution improves as the condenser aperture is increased. The maximum spatial frequency in the image ($m'_{\max}$) is equal to 2 for any value of S. For $S > 1$, however, no increase in the cut-off of $C(m;0)$ above 2 occurs.

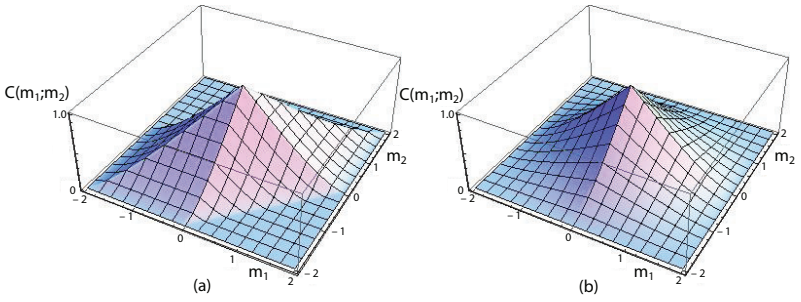

Figure 1. (**a**) The TCC ($C(m_1;m_2)$) for an aberration-free system with a circular objective and condenser pupils for $S = 1$. (**b**) The TCC for a confocal system with two equal circular, aberration-free pupils given by the product of the CTFs of the two lenses, i.e., $c(m_1)c(m_2)$.

For a confocal microscope, the system is coherent, and the TCC separates, so for line structures, for a system with two equal circular pupils,

$$C(m_1;m_2) = \Lambda(|m_1|)\Lambda(|m_2|), \tag{5}$$

as shown in Figure 1b. The maximum spatial frequency in the image ($m'_{\max} = 4$) is twice as high as in a conventional microscope, which is consistent with the point-spread function being $\approx\sqrt{2}$ narrower.

5. Internal Dark Field with Coherent Illumination

Internal dark field is a dark-field method where zero-order light can enter the objective but is blocked by a mask in a Fourier plane. In general, the illumination is incident at an oblique angle but along the optical axis for the special case of central dark field (CDF). In the case of oblique internal dark field, coherent illumination is combined with a stop in the back focal plane of the objective. As imaging is coherent, the TCC is the product of two CTFs, i.e., $C(m_1; m_2) = c(m_1)c^\star(m_2)$. Each CTF ($c(m)$) is constant within its cut-off. For offset illumination, the TCC shifts in the m direction as shown in Figure 2 and can be separated into even and odd components, giving the amplitude and differential phase contrast (DPC), respectively. The total image intensity is the sum of these two components. For CDF (Figure 2a), the TCC is purely even, so there is no odd part and no DPC image. For oblique internal dark field (Figure 2b), the odd part is cancelled in the region of overlap of the two offset squares, while the even part is doubled, so DPC imaging is restricted to the L-shaped regions shown in grey shading. For external dark field (Figure 2c,d), there is no overlap region and no non-zero coverage in the quadrants where m_1 and m_2 are of opposite sign. For oblique internal dark field, as the illumination approaches the edge of the objective pupil, the non-zero coverage in these quadrants tends to disappear. The maximum spatial frequency in the image is $m'_{\max} = 2$ for any value of offset.

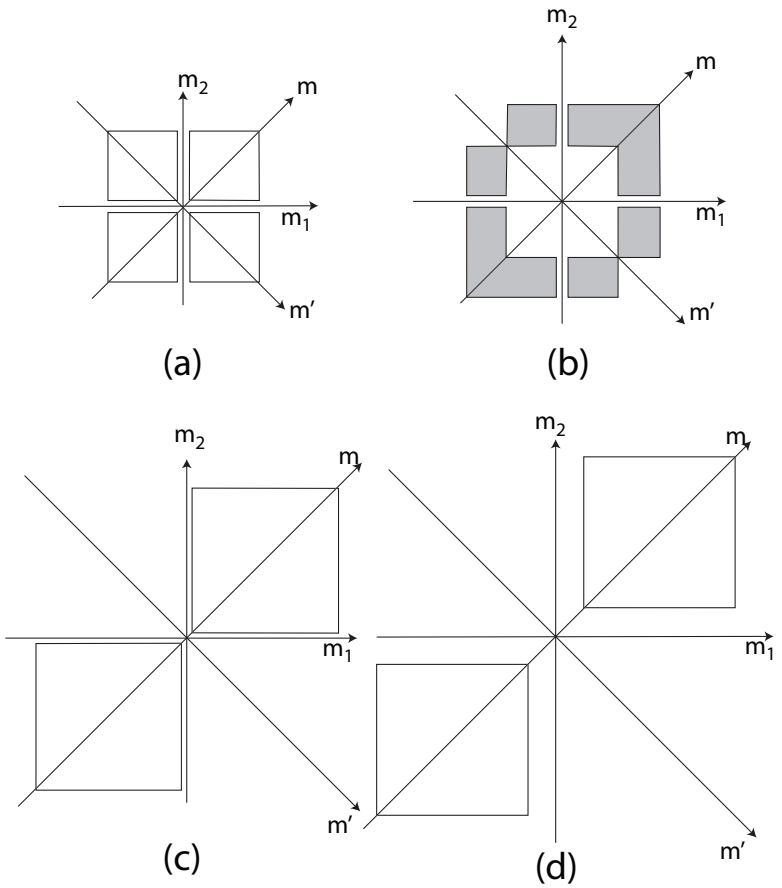

Figure 2. The cut-offs of the TCC for a dark-field system with coherent illumination and a stop in the back focal plane of the objective: (**a**) central dark field (purely even); (**b**) oblique internal dark field (odd component shaded); (**c**) illumination just outside the rim of the objective aperture (cut-offs for both even and odd parts are the same); (**d**) external dark field. For a dark-field system, $C(m, 0) = 0$ for all cases. The maximum spatial frequency in the image is $m'_{\max} = 2$ for all cases but corresponds to different values of the central frequency (m). Although the spatial frequency coordinates (m_1, m_2) are two spatial frequencies in the same (x) direction, they are plotted as Cartesian coordinates. The coordinate axes (m_1, m_2) are rotated and scaled to give axes m' and m.

However, the intensity image is calculated more easily as the squared modulus of the amplitude image.

6. Symmetry of the TCC and PSI-Window

The aberration-free TCC and PSI-window for line structures satisfy different symmetries for different imaging conditions. In all cases, we require that $C(m_1; m_2) = C^*(m_2; m_1)$ so that $C'(m; m') = C^{'*}(m; -m')$ to ensure positivity of intensity. More general cases can be written as sums of components satisfying different symmetry conditions. The different cases are illustrated in Figure 3. Often, the symmetry is more obvious in the coordinates $(m; m')$.

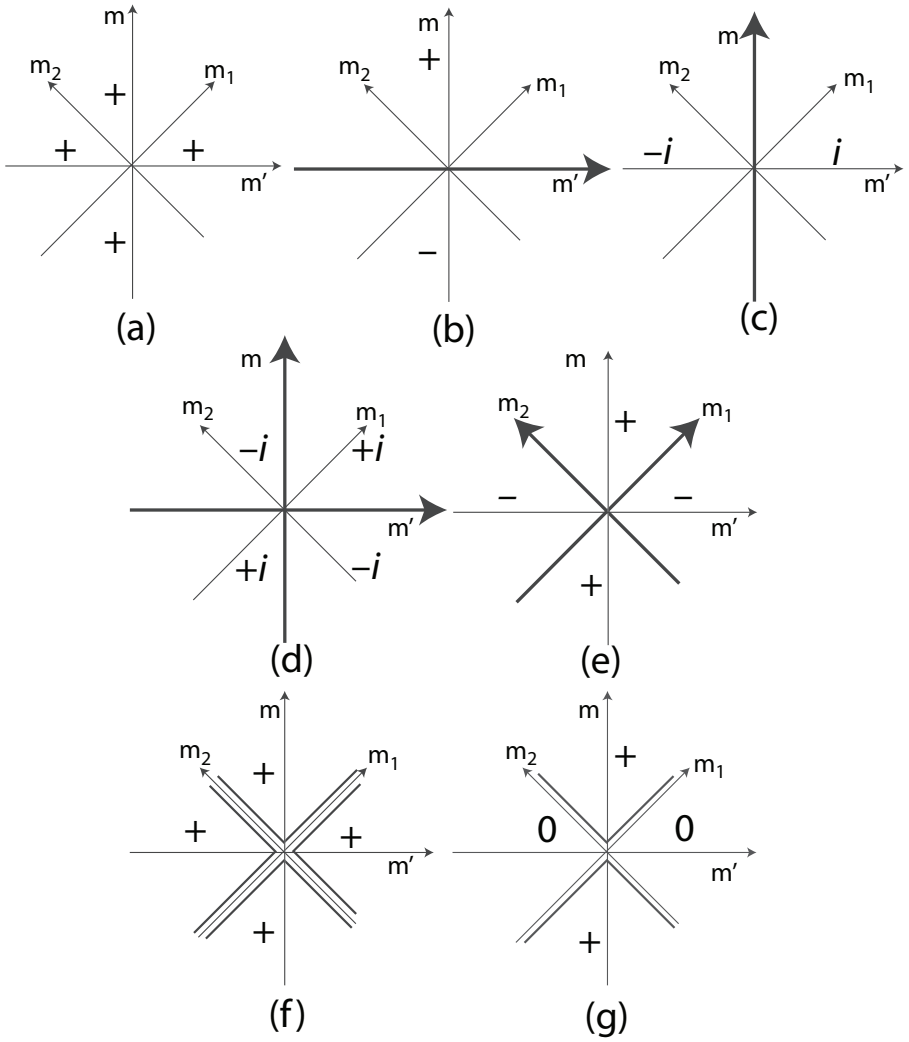

Figure 3. The symmetry of the TCC and the PSI-window, as well as a rotated and scaled TCC, for different imaging conditions. In all cases, $C(m_2; m_1) = C^*(m_1; m_2)$ to ensure that intensity is real. (**a**) Amplitude contrast (AC); (**b**) differential phase contrast (DPC); (**c**) differential amplitude contrast (DAC); (**d**) phase contrast; (**e**) differential contrast (DC); (**f**) central dark field (CDF); (**g**) annular dark field (ADF).

In addition to the first-order relationships, i.e.,

$$\begin{aligned} m_1 + m_2 &= 2m, \\ i(m_1 - m_2) &= im', \end{aligned} \tag{6}$$

the following second-order relationships between the coordinates are useful:

$$\begin{aligned} i(m_1^2 - m_2^2) &= 2imm', \\ m_1^2 + m_2^2 &= 2m^2 + m'^2/2 \\ 2m_1 m_2 &= 2m^2 - m'^2/2. \end{aligned} \tag{7}$$

6.1. Amplitude Contrast (AC)

For AC, $C'(m;m') = C'(m;-m') = C'(-m;m') = C'(-m;-m')$ are real. Also, $C(m_1;m_2) = C(-m_1;-m_2)$.

If the system is also coherent, $C(m_1;m_2) = C(-m_1;m_2) = C(m_1;-m_2) = C(-m_1;-m_2)$.

For the idealised case when the PSI-window is constant and unity for all $(m;m')$, the resulting perfect image of the object ($t = ae^{i\phi}$) is $I = a^2$, and the intensity image is such that phase ϕ is not imaged at all . However, if the PSI-window is of finite size, phase information can be imaged, although weakly. Have changed slightly.

6.2. Differential Phase Contrast (DPC)

For DPC, $C'(m;m') = C'(m;-m') = -C'(-m;m') = -C'(-m;-m')$ are real. Therefore, $C'(m;m')$ is odd in m, and $C'(m;m') = 0$ for $m = 0$.

For a slowly varying object such that $m' = 0$, for the idealised case when the PSI-window is equal to m for all m, the resulting image is $I = a^2 \mathrm{d}\phi/\mathrm{d}v$, i.e., an intensity-weighted differential phase contrast.

DPC is achieved using oblique illumination, as in schlieren imaging [17]. In this case, the DPC image is accompanied by an AC component. The AC component can be subtracted out using successive semicircular illuminations [30] or a split detector in a scanning system [31–35]. In this case, as DPC can give negative signal values, for observation, it must be added to a positive offset.

DIC also gives a DPC image component, the relative strength of which depends on the compensator setting. The components can be separated using phase-shifting DIC [36–39].

6.3. Differential Amplitude Contrast (DAC)

For DAC, $C'(m;m') = -C'(m;-m') = C'(-m;m') = -C'(-m;-m')$ are imaginary. Therefore, $C'(m;m')$ is odd in m', and $C'(m;m') = 0$ for $m' = 0$.

For the idealised case when the PSI-window is proportional to im' for all $(m;m')$, the resulting image is the differential of the intensity image, i.e., $I = \mathrm{d}(a^2)/\mathrm{d}v$. Again, phase is not imaged. For a weak object, $a = 1 + \delta a$, and $I = 2\mathrm{d}(\delta a)/\mathrm{d}v$, which is an image of the differential of the object amplitude transmittance.

If $C'(m;m') = m'^2$, the image is the negative of the second differential of the intensity transmittance, which we call DAC^2. Adding a DAC^2 signal to AC increases the sharpness of the image, as in the case of a Laplacian filter or the unsharp masking technique of photography.

If an image is shifted in a transverse direction by a small, normalised distance (Δ), the TCC is multiplied by a factor of $\exp(-im'\Delta) \approx 1 - i(m_1 - m_2)\Delta$. Therefore, we see that a shift introduces a TCC component with the symmetry of DAC.

6.4. Phase Contrast (PC)

For PC, $C'(m;m') = -C'(m;-m') = -C'(-m;m') = C'(-m;-m')$ are imaginary. Therefore, $C'(m;m') = 0$ for $m = 0$ or $m' = 0$.

For a weak phase object ($t \approx a + ia\phi$),

$$C(m_1;m_2) = \frac{1}{2}[C(m_1;0)\delta(m_2) + C(0,m_2)\delta(m_1)], \tag{8}$$

where $C(m_1;0)$ is imaginary and odd and $C(0,m_2) = C^*(m_1;0)$, resulting in weak-phase imaging. The idealised case when $C(m_1;0) = 1$ and $m_1 \neq 0$ gives perfect weak-phase imaging.

Another case that satisfies this symmetry is $C'(m;m') = imm'$, so $C(m_1;m_2) = i(m_1^2 - m_2^2)/2$, equivalent to a defocused system, which is well known to result in phase contrast and the basis of the transport of intensity method of quantitative phase imaging [40–42].

The imaginary part of the TCC for Zernike phase contrast, using annular illumination and a phase ring, also obeys this symmetry [43].

6.5. Differential Contrast (DC)

For true DC, $C(m_1;m_2) = C(-m_1;-m_2) = -C(-m_1;m_2) = -C(m_1;-m_2)$ are real. Therefore, $C(m_1;m_2) = 0$ for $m_1 = 0$ or $m_2 = 0$.

This symmetry arises for a coherent system with an objective with an odd pupil function. For the idealised case when the TCC is equal to $m_1 m_2$ for all $(m_1;m_2)$, the object amplitude is differentiated, and the resulting image is $I = |\mathrm{d}t/\mathrm{d}v|^2$ or, for a pure phase object, $I = a^2|\mathrm{d}\phi/\mathrm{d}v|^2$ [44]. The nonlinear nature of the imaging results in frequency-doubling artefacts.

A similar effect also occurs in differential interference contrast (DIC) with bias set to extinction, where the overall TCC is that of the microscope itself multiplied by an odd function of m_1 and of m_2 [45]. As the bias is increased, the proportions of DPC and AC components increase, while the proportion of DC decreases.

The OTF for a circular lens exhibits a cusp at the origin, so the TCC may also have a cusp. The cusp in the OTF results in a slow decay in the image of a point or an edge. In general, the PSI-window can be considered to be the product of a PSI-window with a cusp and a smooth function that can be expanded in a power series in $(m;m')$ about the origin (or the TCC in $(m_1;m_2)$). The first-order terms represent DPC and DAC components, in addition to the AC component. Note that the cusp, a discontinuity of slope, disappears in the first order, becoming a discontinuity in curvature. The second-order terms can be represented as sums of components in different ways, choosing from: DC (in $(m_1 m_2)$), DAC^2 (in $(m_1 - m_2)^2 = m'^2$), PC (in $(m_1^2 - m_2^2) = 2mm'$), $(m_1 + m_2)^2/4 = m^2$, and $(m_1^2 + m_2^2)$. For $C'(m;0) = m^2$, with a slowly varying object, the signal is weighted by the value of $C'(m;0)$, so $I = a^2(\mathrm{d}\psi/\mathrm{d}v)^2$, and the sign of the phase derivative is lost.

In DIC, the image is a coherent sum of two mutually shifted, partially coherent images [34,45–47], so the conventional TCC is multiplied by a factor as follows:

$$\begin{aligned}\sin(m_1\Delta + \psi)\sin(m_2\Delta + \psi) &= \frac{1}{2}\left[\sin 2m\Delta \sin 2\psi + \cos m'\Delta - \cos 2m\Delta \cos 2\psi\right] \\ &= \frac{1}{2}\sin 2m\Delta \sin 2\psi + \cos m_1\Delta \cos m_2\Delta \sin^2\psi + \sin m_1\Delta \sin m_2\Delta \cos^2\psi, \quad (9)\end{aligned}$$

where 2Δ is the shear, measured in optical coordinates, and 2ψ is the bias. The total image signal is given by three terms. The first term of the second or last lines (odd in m) represents DPC, and the final term of the last line is DC (odd in m_1 and m_2). The remaining term in the last line, even in m_1 and m_2, or in m' and m, is amplitude contrast (including AC and higher-order AC terms).

For a small bias, the AC component is weak, giving a relatively strong and linear visual DPC, but there is still a DC component of order Δ^2 in strength. The choice of the value of Δ is a compromise between the intensity of the DPC signal and the strength of the spurious DC component. Choosing $\psi \geq 2\Delta$ ensures that there are no zeros in the total TCC within the pass band.

A bias of $\psi = \pi/4$ maximises the DPC signal and makes the DC term zero, but there is still an AC component that reduces the contrast of the DPC term. This is the preferred ap-

proach for digital imaging, as the AC background can be subtracted electronically [45,48,49]. Then, the high-spatial-frequency response for weak phase information is maximised for $\Delta = \pi/4$. However, the PGTF, given by $C'(m;0) = C(m_1;m_1)$, then exhibits a zero value-within the pass band, which could interfere with the performance of the shadow-casting and highlighting relief appearance of the total DIC image.

In a previous paper, we claimed that the TCC for DIC included DAC (in im) and PC (in imm') components [34], but these resulted from the shift effect of the choice of coordinate system and are not really required [45,46].

6.6. Central Dark Field (CDF)

CDF satisfies the same symmetry condition as AC, but as imaging is coherent, $C(m_1;m_2) = C(-m_1;m_2) = C(m_1;-m_2) = C(-m_1;-m_2)$. Also, for dark field, $C(m_1;0) = C(0;m_2) = 0$ so that $C'(m;2m) = C'(m;-2m) = 0$.

6.7. Annular Dark Field (ADF)

For ADF, as for AC, $C'(m;m') = C'(m;-m') = C'(-m;m') = C'(-m;-m')$. Also, $C(m_1;m_2) = 0$ for $m_1 \geq 0 \,\&\, m_2 \leq 0$ or $m_1 \leq 0 \,\&\, m_2 \geq 0$ so that $C'(m;m') = 0$ for $|m'| \geq 2|m|$.

7. Imaging of Phase Objects

Most descriptions of phase imaging are based on a weak object approximation [17]. Scattered light is in phase quadrature to the incident light, which is usually assumed not to be depleted by the interaction. For the amplitude transmittance of a pure-phase object, we have $t = e^{i\phi} \approx 1 + i\phi$. A perfect image then has an intensity of $I = |e^{i\phi}|^2 = 1$, as it is nonabsorbing, but the weak object theory predicts $I = 1 + \phi^2$, which contravenes the principle of conservation of energy. The simple weak object theory is therefore not exact but is nevertheless sufficient to explain the principle of Zernike phase contrast. In order to visualise a weak-phase object, the imaging system must be imperfect in some way, and in general, we should employ a more accurate theory.

We consider the case of an object where the optical path varies with a single cosinusoidal variation, i.e.,

$$t(v) = \exp(ib\cos m_0 v), \tag{10}$$

where the constant (b) determines the strength of modulation. This expression can be used to model an object of constant refractive index whose thickness varies cosinusoidally or, alternatively, an object of constant thickness whose refractive index varies cosinusoidally. From a power-series expansion, we obtain

$$t(v) = \sum_{j=-\infty}^{\infty} i^j J_j(b) e^{ijm_0 v}. \tag{11}$$

Taking the Fourier transform, we obtain an infinite series of discrete spatial frequencies, only some of which will be transmitted through the microscope system. Interestingly, this procedure is well known in the theory of frequency modulation (FM) in communications.

For small values of b, the strength of the image terms decreases for higher powers of b, so the lowest order dominates. We include terms up to the fourth order in b, which is sufficient to give predictions of image intensity to within about 1% for $b \leq 0.5$. This compares with the weak object theory, where $b \leq 0.1$ for the same accuracy. For coherent bright-field systems, truncation of the Fourier components can produce spurious predictions as a result of a Gibbs-like phenomenon.

Expanding the Bessel functions as power series and converting to multiple angles, up to order b^4, we have

$$t(v) = \left(1 - \frac{b^2}{4} + \frac{b^4}{64}\right) + ib\left(1 - \frac{b^2}{8}\right)\cos m_0 v - \frac{b^2}{4}\left(1 - \frac{b^2}{2}\right)\cos 2m_0 v - \frac{b^3}{24}\cos 3m_0 v + \frac{b^4}{192}\cos 4m_0 v. \quad (12)$$

8. Imaging of Phase Objects in Coherent Systems

As examples, in Figure 4, we show the images for phase gratings with quite a large value of $b = 0.5$ for in-focus, coherent, centrally illuminated systems. The plots show one period of the grating structure so that a perfect image of the phase would exhibit maxima at $m_0 v/2\pi$ equal to 0 and 1 and a minimum at 0.5. In Figure 4a, we show the calculated images for a bright-field system that collects harmonics up to $\pm 4m_0$, so the object spatial frequency is in the range of $0 < m_0 < 1/4$. As the object is a pure-phase object, the image in a perfect bright-field system is just a constant value of unity. The red dashed line shows the image calculated from Equation (11) for the first four harmonics, showing that the intensity is very close to unity. Dashed lines are used for the Bessel expansion (Equation (11)), which is exact in the paraxial scalar approximation for a particular number of collected components. The green solid line shows the image calculated from the power-series expansion of t to the fourth order in Equation (12), showing that the prediction is still good. The orange dashed line uses the Bessel expansion for two harmonics. This predicts the correct image for object spatial frequencies in the range of $1/3 < m_0 < 1/2$ and shows that this phase object is imaged as a frequency-doubled, second-harmonic variation in intensity. The global maxima in the image intensity correspond to the regions of zero-phase gradient. This is understandable, as a phase gradient deflects the illuminating light so that some power is rejected. However, for lower object-grating frequencies in the range of $0 < m_0 < 1/4$, the Bessel expansion for two harmonics predicts a higher-intensity variation than really occurs, although it remains within 1% accuracy. A similar effect occurs for object frequencies in the band of $1/4 < m_0 < 1/3$, but now, the Bessel expansion predicts a fourth-harmonic image variation. The blue solid line shows the result of calculation by a power-series expansion of t to the second order in b. In this case, the predicted intensity is larger and does not satisfy conservation of energy, demonstrating that the second-order expansion may not always be valid. These results indicate that for coherent bright field, different bands of object spatial frequency are imaged differently according to the harmonic components that contribute to the image. Therefore, for a phase object with a mixture of object spatial frequencies, the image may be difficult to interpret. However, high object frequencies such that $1/2 < m_0 < 1$ will dominate in the image.

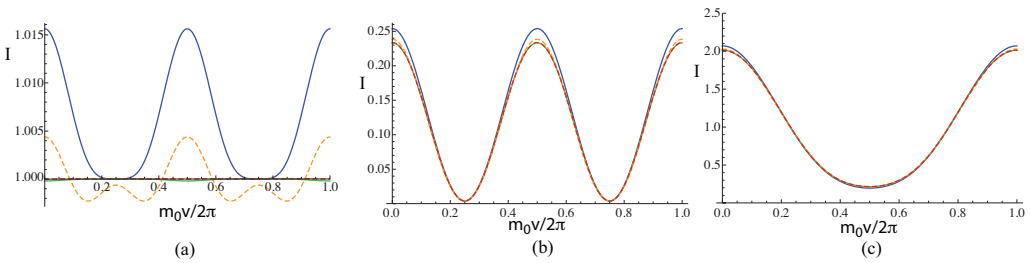

Figure 4. Calculated intensity (I) images of a phase grating with $b = 0.5$. (**a**) Bright field. (**b**) Central dark field (CDF). (**c**) Phase contrast. Dashed lines refer to calculation using the Bessel functions to the fourth harmonic (red) and second harmonic (orange). Solid lines correspond the power-series expansion to the fourth order (green) and second order (blue). A bright-field image with no object would result in an image intensity of unity.

In Figure 4b, we show the results for a central dark-field (CDF) system. Now, the two calculations to the fourth harmonic give similar results, but the two second-harmonic expansions are a little different, with the second-order power-series expansion not meeting 1% accuracy. All the curves show the same shape: a frequency-doubled image of the phase variation. In Figure 4c, we show the results for a phase-contrast system in which the direct beam is phase-shifted by 90°. All the calculated curves agree quite well and show a first-harmonic image, agreeing in shape with the object phase variation but with the second-order power-series expansion not meeting 1% accuracy.

Figure 5 shows the effect of offset illumination in a coherent bright-field system that collects harmonics up to $4m_0$. If the offset is sufficient to eliminate just the negative fourth-harmonic component, the image intensity predicted by the Bessel fourth-harmonic theory, shown in Figure 5a, now predicts a quadrupled-frequency, fourth-harmonic image. The fourth-order power-series theory gives a reasonable agreement. The second-order theories give poor predictions if the grating frequency is in the range of $0 < m_0 < 1/4$. If the offset is larger, to eliminate the negative third and fourth harmonics (Figure 5b), the two fourth-order theories give very similar results, showing third-harmonic intensity variation and exhibiting a transverse image shift. If the offset eliminates the negative second to fourth harmonics (Figure 5c), we see a second-harmonic image-intensity variation. The second-order theories predict qualitatively correct images. If the offset eliminates the negative first to fourth harmonics (Figure 5d), all four theories give consistent results, showing a strong image of the phase derivative on a constant background. These results show that a coherent bright-field system with sufficient offset can result in good DPC images of phase structures.

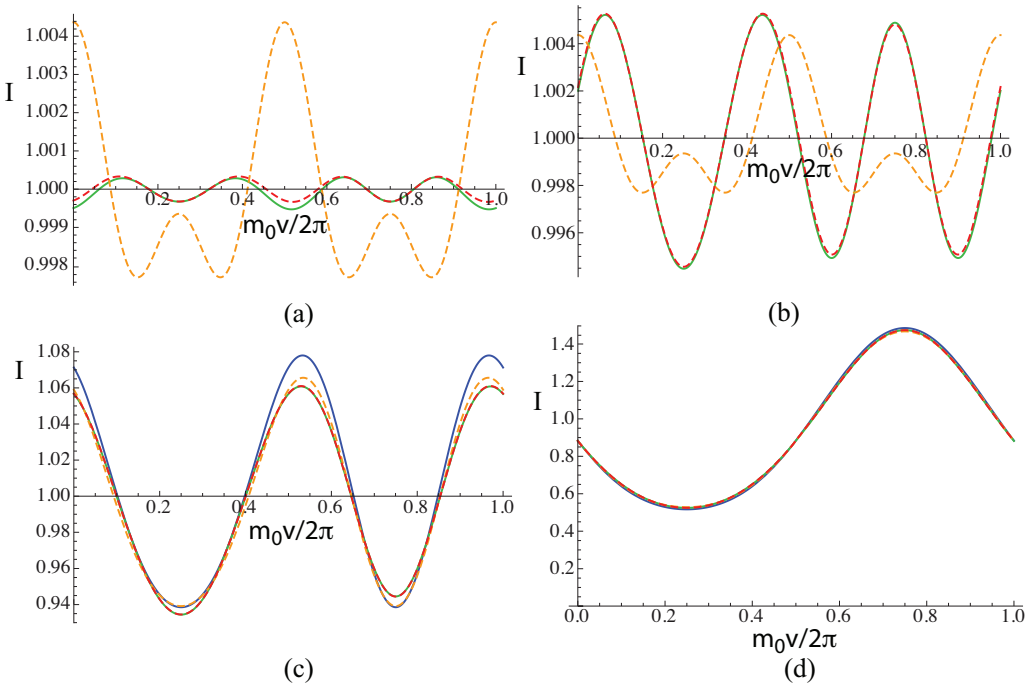

Figure 5. Calculated intensity (I) images of a phase grating with $b = 0.5$ for bright-field offset illumination. (**a**) Offset sufficient to eliminate the negative fourth harmonic. (**b**) Offset sufficient to eliminate negative third and fourth harmonics. (**c**) Offset sufficient to eliminate negative second to fourth harmonics. (**d**) Offset sufficient to eliminate negative first to fourth harmonics. Dashed lines refer to calculation using the Bessel functions to the fourth harmonic (red) and second harmonic (orange). Solid lines correspond to power-series expansion to the fourth order (green) and second order (blue). A bright-field image with no object would result in an image intensity of unity.

Figure 6 shows the effects of an offset in a coherent dark-field system that collects harmonics up to $4m_0$. This is an internal dark-field arrangement. A small offset results

in a negligible change in the image. Figure 6a shows the result for an offset sufficient to eliminate negative second to fourth harmonics, with the results still agreeing quite well with Figure 4b. Figure 6b shows the result for an offset sufficient to eliminate negative first to fourth harmonics. Now, we see a DPC image of the grating but weaker than in the bright-field case in Figure 5d. This behaviour is caused by an optical amplification effect of the zero-order beam in the bright-field case [50], just as in interference scattering (iSCAT) microscopy [51].

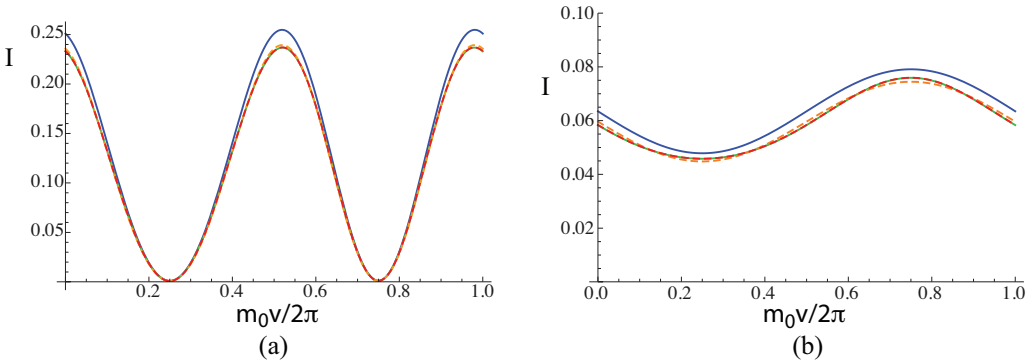

Figure 6. Calculated intensity (I) images of a phase grating with $b = 0.5$ for dark-field offset illumination. (**a**) Offset sufficient to eliminate negative second to fourth harmonics. (**b**) Offset sufficient to eliminate negative first to fourth harmonics. Dashed lines refer to calculation using the Bessel functions to the fourth harmonic (red) and second harmonic (orange). Solid lines correspond to power-series expansion to the fourth order (green) and second order (blue). A bright-field image with no object would result in an image intensity of unity.

Figure 7 shows the effects of an offset in a coherent phase-contrast system that collects harmonics up to $4m_0$. Again, a small offset results in a negligible change in the image. Figure 7a shows the result for an offset sufficient to eliminate negative second to fourth harmonics, with the results agreeing quite well with Figure 4c, although there is a small asymmetry and a transverse shift. Figure 7b shows the result for an offset sufficient to eliminate negative first to fourth harmonics. Now, there is a stronger asymmetry and a larger transverse shift. These effects are caused by an interaction between phase contrast and differential phase-contrast mechanisms.

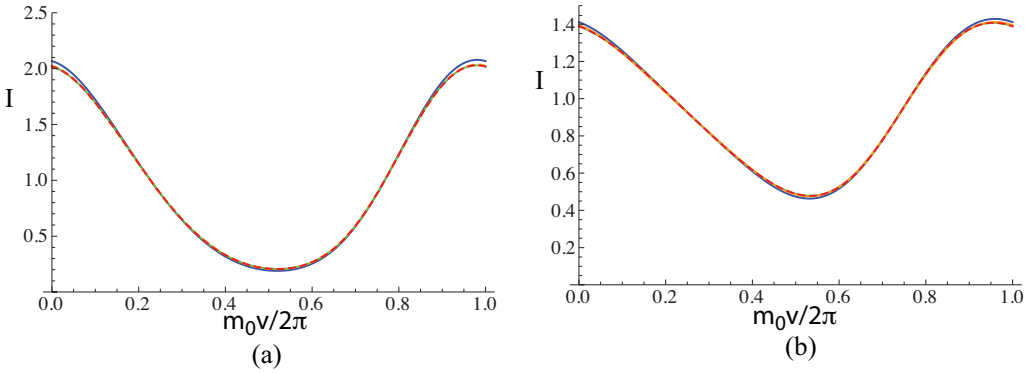

Figure 7. Calculated intensity (I) images of a phase grating with $b = 0.5$ for phase-contrast offset illumination. (**a**) Offset sufficient to eliminate negative second to fourth harmonics. (**b**) Offset sufficient to eliminate negative first to fourth harmonics. Dashed lines refer to calculation using the Bessel functions to the fourth harmonic (red) and second harmonic (orange). Solid lines correspond to power-series expansion to the fourth order (green) and second order (blue). A bright-field image with no object would result in an image intensity of unity.

This section has shown that calculation of images of phase gradients in bright-field systems is complicated and may require the inclusion of terms up to the fourth harmonic

of the object grating frequency. For dark field or phase contrast, second harmonic terms are usually sufficient to achieve at least qualitatively correct image prediction.

9. Imaging of Phase Objects in Partially Coherent Systems

We now compare the imaging performance for phase objects of partially coherent systems with TCCs that exhibit various different symmetry properties.

9.1. Amplitude Contrast (AC)

We have already described how $C(m_1;m_2) = C^*(m_2;m_1)$ in order to producea real intensity image. For an aberration-free (and in-focus), axially symmetrical system, $C(-m_1;-m_2) = C(m_1;m_2)$. In this case, we need only consider particular spatial frequencies for positive values of m_1 and $m_1 \geq |m_2|$, corresponding to positive values of $(m;m')$, with the remaining terms following from symmetry considerations. The image intensity for a phase object with a single cosinusoidal variation in optical path is

$$I(v) = a_0 + a_2 \cos 2m_0 v + a_4 \cos 4m_0 v + \ldots, \tag{13}$$

where the odd terms are $a_1 = a_3 = \cdots = 0$, and expanding the Bessel functions as power series in a as follows:

$$\begin{aligned} a_0 &= C(0;0) - \tfrac{1}{2}[C(0;0) - C(m_0;m_0)]b^2 \\ &\quad + \frac{1}{32}[3C(0;0) - 4C(m_0;m_0) + C(2m_0;2m_0)]b^4 + \ldots \\ a_2 &= \frac{1}{2}[C(m_0;-m_0) - C(2m_0;0)]b^2 \\ &\quad - \frac{1}{24}[3C(m_0;-m_0) - 4C(2m_0;0) + C(3m_0;m_0)]b^4 + \ldots \\ a_4 &= \frac{1}{96}[3C(2m_0;-2m_0) - 4C(3m_0;-m_0) + C(4m_0;0)]b^4 + \ldots \end{aligned} \tag{14}$$

As the image of a phase object is only of magnitude order b^2 but amplitude information is imaged as order b, we call this amplitude contrast (AC). The dominant term in order b^2 for a_2 consists of a difference frequency and a second-harmonic weak object component. If all the frequency components are transmitted through the system, the terms in order b^2 for a_2 and b^4 for a_4 vanish for a conventional bright-field microscope with $S = 1$, as $C(m_0;-m_0) = C(2m_0;0)$ and $[3C(2m_0;-2m_0) - 4C(3m_0;-m_0) + C(4m_0;0)] = 0$. There is no $\cos 2m_0 v$ image to order b^2 in this case. A similar effect occurs for a coherent system, i.e., $S = 0$. In this case, the b^4 term in a_2 can also be zero. Therefore, a bright-field system effectively acts as a band-pass filter for phase information. In order to image phase objects efficiently, the symmetry of the TCC must be altered, which we now discuss.

9.2. Differential Phase Contrast (DPC)

For differential phase contrast (DPC), $C(-m_1;-m_2) = -C(m_1;m_2)$; therefore, $C'(-m;m') = -C'(m;m')$. There is no constant term, i.e., $a_0 = 0$, so the intensity can take negative values. A constant value can be added for display purposes. The image intensity is

$$I(v) = a_1 \sin m_0 v + a_3 \sin 3m_0 v + \ldots, \tag{15}$$

where

$$\begin{aligned} a_1 &= 2C(m_0;0)b - \tfrac{1}{4}[3C(m_0;0) - C(2m_0;m_0)]b^3 + \ldots \\ a_3 &= \frac{1}{12}[3C(2m_0;-m_0) - C(3m_0;0)]b^3 + \ldots \end{aligned} \tag{16}$$

The differential phase image is of magnitude order b. If the value of $C(m;m)$ increases linearly in m from the origin, then the terms of both a_1 and a_3 in b^3 cancel, giving an image proportional to the phase differential, i.e., with sine rather than cosine variation.

9.3. Differential Amplitude Contrast (DAC)

For differential amplitude contrast (DAC), the TCC is taken as $iC(m_1;m_2)$ for $m_1 > m_2$ (positive m'), with $C(m_1;m_2)$ being real, so it becomes $-iC(m_1;m_2)$ for $m_1 < m_2$ (negative m'). Then,

$$I(v) = a_2 \sin 2m_0 v + a_4 \sin 4m_0 v + \dots, \tag{17}$$

where

$$\begin{aligned} a_2 =& \tfrac{1}{2}[C(2m_0;0) - C(m_0;-m_0)]b^2 \\ &+ \frac{1}{24}[3C(m_0;-m_0) - 4C(2m_0;0) + C(3m_0;m_0)]b^4 + \dots \\ a_4 =& -\frac{1}{96}[3C(2m_0;-2m_0) - 4C(3m_0;-m_0) + C(4m_0;0)]b^4 + \dots \end{aligned} \tag{18}$$

There is no first-harmonic $\sin m_0 v$ term for a phase object and no image of order b in strength. DAC gives a differential amplitude image for weak-amplitude objects, as the WOTF is imaginary and odd [44].

9.4. Phase Contrast (PC)

Zernike phase contrast has a WOTF that is imaginary and even, superposed on a positive $C(0;0)$ [52], the strength of which depends on the absorption of the phase ring. There is also an additional annular dark-field component for annular phase contrast [46]. We generalise this symmetry for the WOTF so that for $m_1 > 0$ & $m_1 > |m_2|$, the TCC is $iC(m_1;m_2)$, where $C(m_1;m_2)$ is real, as well as for $m_1 < 0$ & $|m_1| > |m_2|$. Then, the TCC for phase contrast (PC) is $-iC(m_1;m_2)$ for $m_2 > 0$ & $m_2 > |m_1|$, as well as for $m_2 < 0$ & $|m_2| > |m_1|$. In terms of the variables $(m;m')$, it is $iC(m_1;m_2)$ if $(m;m')$ have the same sign or $-iC(m_1;m_2)$ if they have opposite signs. Then,

$$I(v) = a_0 + a_1 \cos m_0 v + a_3 \cos 3m_0 v + \dots, \tag{19}$$

where

$$\begin{aligned} a_0 =& C(0;0) \\ a_1 =& 2C(m_0;0)b + \frac{1}{4}[3C(m_0;0) - C(2m_0;m_0)]b^3 + \dots \\ a_3 =& \frac{1}{12}[3C(2m_0;-m_0) - 4C(3m_0;0)]b^3 + \dots . \end{aligned} \tag{20}$$

9.5. Differential Contrast (DC)

For true differential contrast (DC), the TCC is $C(m_1;m_2)$ for m_1 and m_2 of the same sign, and $C(m_1;-m_2) = C(-m_1;m_2) = -C(m_1;m_2)$ [44]. As $C(m_1;0) = 0$, weak objects are not imaged.

For true DC, in Equation (13), we have

$$\begin{aligned} a_0 =& \tfrac{1}{2}C(m_0;m_0)a^2 - \frac{1}{32}[4C(m_0;m_0) - C(2m_0;2m_0)]b^4 + \dots \\ a_2 =& \tfrac{1}{2}C(m_0;m_0)b^2 - \frac{1}{24}[3C(m_0;m_0) + C(3m_0;m_0)]b^4 + \dots \\ a_4 =& \frac{1}{96}[3C(2m_0;2m_0) - 4C(3m_0;m_0)]b^4 + \dots, \end{aligned} \tag{21}$$

so the image is of order b^2 in strength, unlike DPC and PC, which both give images of order b.

For the similar effect in differential interference contrast (DIC) with bias set to extinction, i.e., $\psi = 0$, $C(m_1; -m_2) = C(-m_1; m_2) \neq -C(m_1; m_2)$, and

$$\begin{aligned} a_0 &= \tfrac{1}{2}C(m_0; m_0)a^2 - \frac{1}{32}[4C(m_0; m_0) - C(2m_0; 2m_0)]b^4 + \ldots \\ a_2 &= -\tfrac{1}{2}C(m_0; -m_0)b^2 + \frac{1}{24}[3C(m_0; -m_0) - C(3m_0; m_0)]b^4 + \ldots \\ a_4 &= -\frac{1}{96}[3C(2m_0; -2m_0) - 4C(3m_0; -m_0)]b^4 + \ldots, \end{aligned} \tag{22}$$

9.6. Central Dark Field (CDF)

The cases of annular and central dark field are special cases of amplitude contrast with some values of the TCC set to zero. In central dark field (CDF), the TCC is zero for $m_1 = 0$ or $m_2 = 0$. Then, in Equation (13),

$$\begin{aligned} a_0 &= \tfrac{1}{2}C(m_0; m_0)b^2 - \frac{1}{32}[4C(m_0; m_0) - C(2m_0; 2m_0)]b^4 + \ldots \\ a_2 &= \tfrac{1}{2}C(m_0; -m_0)b^2 - \frac{1}{24}[3C(m_0; -m_0) + C(3m_0; m_0)]b^4 + \ldots \\ a_4 &= \frac{1}{96}[3C(2m_0; -2m_0) - 4C(3m_0; -m_0)]b^4 + \ldots. \end{aligned} \tag{23}$$

The dominant term in order b^2 for a_2 is a difference frequency component.

9.7. Annular Dark Field (ADF)

The symmetry of Figure 3g arises for a thin annular condenser pupil with an inner radius equal to that of the objective pupil, giving annular dark field (ADF). The TCC is zero when $m_1 = 0$ or $m_2 = 0$, as well as for m_1 and m_2 of opposite sign [9,25]. Then, in Equation (13),

$$\begin{aligned} a_0 &= \tfrac{1}{2}C(m_0; m_0)b^2 - \frac{1}{32}[4C(m_0; m_0) - C(2m_0; 2m_0)]b^4 + \ldots \\ a_2 &= -\frac{1}{24}C(3m_0; m_0)b^4 + \ldots, \\ a_4 &= 0 \times b^4 + \ldots. \end{aligned} \tag{24}$$

and the second-harmonic term (a_2) is only of order b^4. The term in b^2 for a_2 vanishes for annular dark field, as $C(m_0; -m_0) = 0$. The spatial frequency cut-off for annular dark field is twice that for central dark field, but for the former, the response falls off, while for the latter, it is constant up to the cut-off.

This geometry is often used for metallurgical (reflection) microscopes. For a transmission system where the annulus is surrounded by the outer part of the objective pupil, an additional contribution comes from this outer part. This contribution is similar to CDF, except that it is partially coherent rather than coherent.

10. Imaging of Phase Objects with Two Cosinusoidal Components

In the previous section, we considered a single-frequency cosinusoidal variation in optical path and obtained the image intensity to order b^4, resulting in spatial frequencies in the image up to $4m_0$, corresponding to a fourth harmonic. Here, we consider an object with cosinusoidal variations with two frequencies: m_{0A}, m_{0B} and $m_{0A} \geq m_{0B}$, with corresponding amplitudes of b_A and b_B. As there are now sum and difference frequencies of m_{0A} and m_{0B} present, the results to order b^4 consist of many terms, so we restrict the treatment to

order b^2, which is sufficient to predict the image intensity reasonably accurately in most cases, especially as the TCC falls off with spatial frequency.

10.1. Amplitude Contrast (AC)

The image intensity is of the following form:

$$\begin{aligned} I(v) =& a_0 + a_{2A}\cos 2m_{0A}v + a_{2B}\cos 2m_{0B}v \\ &+ a_{A-B}\cos(m_{0A} - m_{0B})v + a_{A+B}\cos(m_{0A} + m_{0B})v \ldots \end{aligned} \tag{25}$$

where

$$\begin{aligned} a_0 =& C(0;0) - \frac{1}{2}[C(0;0) - C(m_{0A};m_{0A})]b_A^2 \\ &- \frac{1}{2}[C(0;0) - C(m_{0B};m_{0B})]b_B^2 + \ldots \\ a_{2A} =& \frac{1}{2}[C(m_{0A};-m_{0A}) - C(2m_{0A};0)]b_A^2 + \ldots \\ a_{2B} =& \frac{1}{2}[C(m_{0B};-m_{0B}) - C(2m_{0B};0)]b_B^2 + \ldots \\ a_{A-B} =& [C(m_{0A};m_{0B}) - C(m_{0A} - m_{0B};0)]b_A b_B + \ldots \\ a_{A+B} =& [C(m_{0A};-m_{0B}) - C(m_{0A} + m_{0B};0)]b_A b_B + \ldots, \end{aligned} \tag{26}$$

so in general, we have sum and difference frequency terms of a_{A+B} and a_{A-B}, in addition to the second harmonics, i.e., a_{2A} and a_{2B}. Each of these terms is made up of sums and differences of the original object frequencies.

10.2. Differential Phase Contrast (DPC)

For DPC,

$$I(v) = a_{1A}\sin m_{0A}v + a_{1B}\sin m_{0B}v + \ldots, \tag{27}$$

where

$$\begin{aligned} a_{1A} =& 2C(m_{0A};0)b_A + \ldots \\ a_{1B} =& 2C(m_{0B};0)b_B + \ldots, \end{aligned} \tag{28}$$

giving linear imaging of the phase differential, as we are now neglecting terms of order b^3.

10.3. Differential Amplitude Contrast (DAC)

For DAC,

$$\begin{aligned} I(v) =& a_{2A}\sin 2m_{0A}v + a_{2B}\sin 2m_{0B}v + a_{A-B}\sin(m_{0A} - m_{0B})v \\ &+ a_{A+B}\sin(m_{0A} + m_{0B})v + \ldots, \end{aligned} \tag{29}$$

where

$$\begin{aligned} a_{2A} =& \frac{1}{2}[C(2m_{0A};0) - C(m_{0A};-m_{0A})]b_A^2 + \ldots, \\ a_{2B} =& \frac{1}{2}[C(2m_{0B};0) - C(m_{0B};-m_{0B})]b_B^2 + \ldots, \\ a_{A-B} =& \frac{1}{2}[C(m_{0A} - m_{0B};0) - C(m_{0A};m_{0B})]b_A b_B + \ldots, \\ a_{A+B} =& \frac{1}{2}[C(m_{0A} + m_{0B};0) - C(m_{0A};-m_{0B})]b_A b_B + \ldots, \end{aligned} \tag{30}$$

consisting of second-harmonic terms and sum and difference frequency terms.

10.4. Phase Contrast (PC)

For PC,

$$I(v) = a_0 + a_{1A}\cos m_{0A}v + a_{1B}\cos m_{0B}v + \ldots \tag{31}$$

where

$$\begin{aligned} a_0 &= C(0;0), \\ a_{1A} &= 2C(m_{0A};0)b_A + \ldots, \\ a_{1B} &= 2C(m_{0B};0)b_B + \ldots, \end{aligned} \tag{32}$$

so for weak objects, phase is imaged linearly.

10.5. Differential Contrast (DC)

For DC, in Equation (25), we have

$$\begin{aligned} a_0 &= \frac{1}{2}C(m_{0A};m_{0A})b_A^2 + \frac{1}{2}C(m_{0B};m_{0B})b_B^2 + \ldots, \\ a_{2A} &= -\frac{1}{2}C(m_{0A};m_{0A})b_A^2 + \ldots, \\ a_{2B} &= -\frac{1}{2}C(m_{0B};m_{0B})b_B^2 + \ldots, \\ a_{A-B} &= -C(m_{0A};m_{0B})b_A b_B + \ldots, \\ a_{A+B} &= -C(m_{0A};m_{0B})b_A b_B + \ldots, \end{aligned} \tag{33}$$

with sum and difference terms of equal strength, and for DIC at extinction, $\psi = 0$,

$$\begin{aligned} a_0 &= \frac{1}{2}C(m_{0A};m_{0A})a_A^2 + \frac{1}{2}C(m_{0B};m_{0B})b_B^2 + \ldots, \\ a_{2A} &= \frac{1}{2}C(m_{0A};-m_{0A})b_A^2 + \ldots, \\ a_{2B} &= \frac{1}{2}C(m_{0B};-m_{0B})b_B^2 + \ldots, \\ a_{A-B} &= -C(m_{0A};m_{0B})b_A b_B + \ldots, \\ a_{A+B} &= C(m_{0A};-m_{0B})b_A b_B + \ldots, \end{aligned} \tag{34}$$

so that, now, the sum and difference frequency terms are, in general, of different strengths.

10.6. Central Dark Field (CDF)

For CDF, in Equation (25),

$$\begin{aligned} a_0 &= \frac{1}{2}C(m_{0A};m_{0A})b_A^2 + \tfrac{1}{2}C(m_{0B};m_{0B})b_B^2 + \ldots, \\ a_{2A} &= \frac{1}{2}C(m_{0A};-m_{0A})b_A^2 + \ldots, \\ a_{2B} &= \frac{1}{2}C(m_{0B};-m_{0B})b_B^2 + \ldots, \\ a_{A-B} &= C(m_{0A};m_{0B})b_A b_B + \ldots, \\ a_{A+B} &= C(m_{0A};-m_{0B})b_A b_B + \ldots, \end{aligned} \tag{35}$$

each frequency is imaged as a second-harmonic term, and sum and difference frequency terms are also present.

10.7. Annular Dark Field (ADF)

For (idealised) ADC in Equation (25),

$$\begin{aligned} a_0 &= \frac{1}{2}C(m_{0A};m_{0A})b_A^2 + \frac{1}{2}C(m_{0B};m_{0B})b_B^2 + \ldots, \\ a_{2A} &= 0 \times b_A^2 + \ldots, \\ a_{2B} &= 0 \times b_B^2 + \ldots, \\ a_{A-B} &= C(m_{0A};m_{0B})b_A b_B + \ldots, \\ a_{A+B} &= 0 \times b_A b_B + \ldots, \end{aligned} \tag{36}$$

and only the difference frequency term appears in the intensity image [9]. This aliased signal is difficult to interpret. In a system with an annular inner radius smaller than the objective radius, the missing second harmonic and sum terms are present but may be misinterpreted in the aliased background. For these reasons, annular darkfield is probably best to be restricted to sparse objects.

11. Partially Coherent Imaging in Particular Systems

11.1. Annular Dark Field

The area of overlap of an infinitely thin annulus and a circle of equal radius is

$$\begin{aligned} \Lambda_{\mathrm{Ann}}(m) &= \frac{2}{\pi}\arccos(m/2), && |m| \le 2 \\ &= 0, && |m| \ge 2. \end{aligned} \tag{37}$$

The value of $\Lambda_{\mathrm{ann}}(0)$ depends critically on the radius of the annulus [53]. If the inner radius is equal to that of the circle, $\Lambda_{\mathrm{ann}}(0) = 0$. If the outer radius is equal to that of the circle, $\Lambda_{\mathrm{ann}}(0) = 2$. If the mean radius of the annulus is approximately equal to that of the circle, we can ensure that $\Lambda_{\mathrm{ann}}(0) = 1$.

For a (idealised) dark-field system with a thin annular condenser with an inner radius equal to that of the objective pupil, for line structures,

$$\begin{aligned} C(m_1;m_2) &= \Lambda_{\mathrm{Ann}}(m_1), && |m_1| \ge |m_2| > 0,\ \mathrm{sgn}\, m_2 = \mathrm{sgn}\, m_1 \\ &= \Lambda_{\mathrm{Ann}}(m_2), && |m_2| \ge |m_1| > 0,\ \mathrm{sgn}\, m_2 = \mathrm{sgn}\, m_1 \\ &= 0, && \mathrm{sgn}\, m_2 = -\mathrm{sgn}\, m_1, \end{aligned} \tag{38}$$

as shown in Figure 8a. This was sketched in Ref. [46]. As with any dark-field system, the WOTF is zero, so a weak object theory is not applicable. The TCC is zero for object frequencies of $\mathrm{sgn}\, m_2 = -\mathrm{sgn}\, m_1$, but not for frequencies of $\mathrm{sgn}\, m_2 = \mathrm{sgn}\, m_1$, which result as frequencies of $m' = m_1 - m_2$ in the image. The maximum spatial frequency in the image is $m'_{\mathrm{max}} = 2$. If the annulus has a mean radius equal to the radius of the objective pupil, the system is no longer a dark-field system, so the WOTF is $C(m_{1,2};0) \neq 0$ (Figure 8b). The high-spatial-frequency response for weak objects is considerably enhanced relative to a system with a circular condenser aperture.

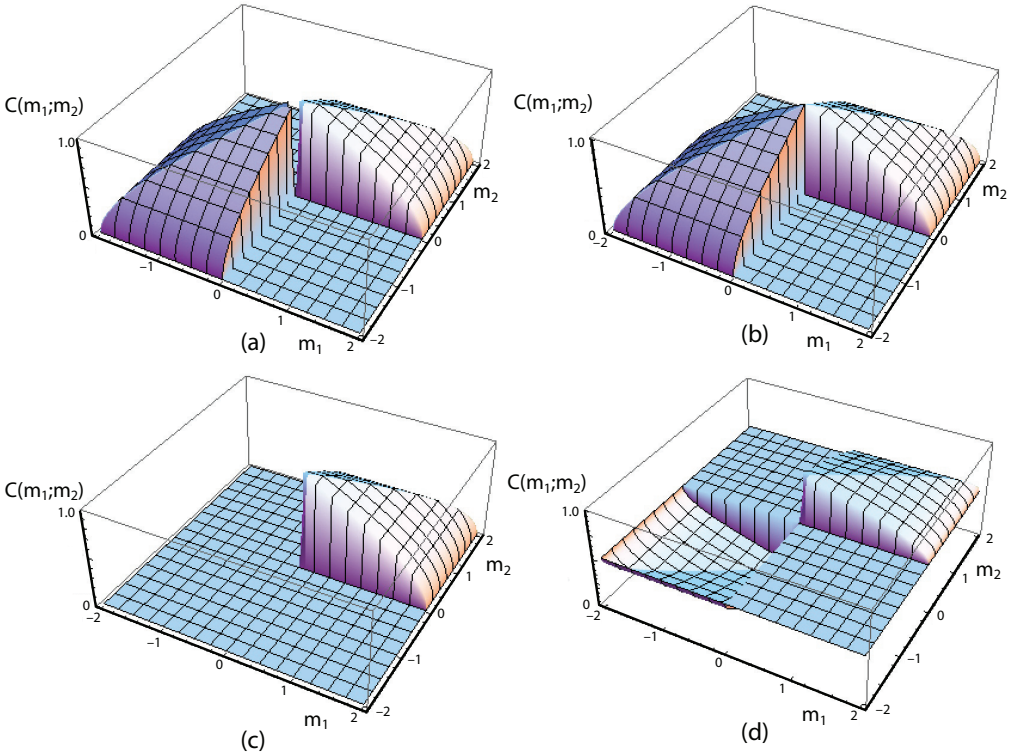

Figure 8. (**a**) The TCC $C(m_1; m_2)$ for line structures for annular dark field, with a thin annular condenser pupil just larger in radius than the objective aperture. The WOTF is $C(m_{1,2}; 0) = 0$. (**b**) If the mean radius of the annulus is equal to the radius of the objective aperture, for the resulting bright-field system, the WOTF is $C(m_{1,2}; 0) \neq 0$. (**c**) The TCC for a thin, semicircular annular condenser pupil just larger in radius than the objective aperture. (**d**) DPC determined by subtracting signals from two thin, semicircular annular condenser pupils. The value of the WOTF, i.e., $C(m_{1,2}; 0)$, depends critically on the radius of the annulus.

11.2. Semicircular Condenser Pupil with Circular Objective Pupil

The TCC for a system with a semicircular condenser pupil and a circular objective pupil of equal radius for line structures varying only in the direction of the narrow dimension of the semicircle is given in Appendix A.1 and shown in Figure 9a.

We see that the WOTF and the PGTF are both equal to $[\Lambda(m) - \frac{1}{2}\Lambda(2m)]$ for $2 \geq m \geq 0$ and $\frac{1}{2}\Lambda(2|m|)$ for $0 \geq m \geq -1$. The PGTF gives the intensity in the image for a phase-gradient object, which decreases monotonically for negative slopes, cutting off at $m_0 = -1$. For small, positive slopes, the intensity is unchanging with slope so that there is no high-lighting, then decreases, cutting off at $m_0 = 2$.

Normal amplitude contrast results if $C'(m; m')$ is real and an even function of m, while a real and odd function of m gives differential phase contrast (DPC) [44]. An imaginary and odd function of m' (in order to maintain the required condition of $C(m_1; m_2) = C^*(m_2; m_1)$) gives differential amplitude contrast, imaging the gradient of amplitude transmittance. Thus, the image for a semicircular condenser pupil and a circular objective pupil gives a mixture of normal amplitude contrast (AC) and DPC. If the signals using two opposing semicircular condenser pupils are added, the DPC term cancels, and we are left with a conventional bright-field system, with the TCC as given in Figure 1a. If the two signals are subtracted, the AC signal cancels, and the resulting DPC has a TCC as shown in Figure 9b. A density plot was shown in Ref. [43]. The TCC is given explicitly in Appendix A.2. We see that the WOTF and the PGTF are both equal to $[\Lambda(m) - \Lambda(2m)]$ for $2 \geq m \geq 0$ and $-\Lambda(|m|) + \Lambda(2|m|)$ for $0 \geq m \geq -2$. Note that the strengths of the $\Lambda(2m_{1,2})$ components differ in the case of a single semicircular condenser pupil.

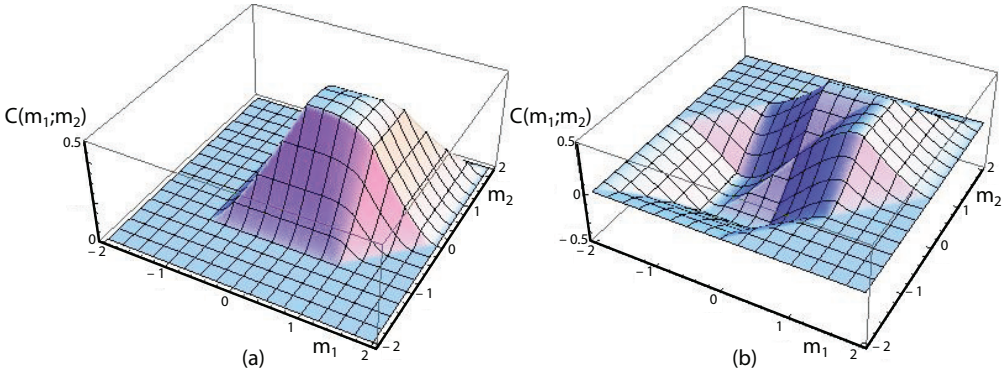

Figure 9. (**a**) The TCC, i.e., $C(m_1; m_2)$, for line structures for a system with a semicircular condenser pupil and a circular objective pupil of equal radius. (**b**) A split-detector system with the signals from the two semicircular elements subtracted to give DPC. This is equal to twice the odd part in m of the TCC in (**a**), giving rise to DPC. The corresponding even part in m results in conventional AC, as shown in Figure 1a.

These results can be modified for cases of a quadrant condenser pupil, an annular split source, or a first-moment (linear ramp) condenser pupil [32,33,35].

By splitting the source into two semicircular regions, we can measure an estimate of the phase gradient in the direction across the narrow dimension of the semicircles (say, the x direction). By estimating the phase gradient in two orthogonal directions (x, y), the phase can be determined [39]. This can be achieved by taking measurements from four source quadrants, where two adjacent quadrants can give a semicircular source in either the x or y orientation.

11.2.1. Quadrant Condenser Pupil

The phase gradient in the directions at $\pm 45^\circ$ can also be estimated using subtraction of signals using two opposite quadrants. Then, for four quadrants, two opposite quadrants can estimate phase gradient in two directions at $\pm 45^\circ$. The $[1 - \Lambda(m)]$ function is an odd function of m. We define a new odd function $(\Omega(m))$ as

$$\begin{aligned} \Omega(m) =& \frac{1}{2}\left[1 - \Lambda(\sqrt{2}m) - \frac{m|m|}{\pi}\right], && |m| \le 2, \\ =& 0, && |m| > 2. \end{aligned} \tag{39}$$

For DPC, some expressions are simplified if we also introduce an odd function related to Λ, i.e.,

$$\begin{aligned} \Upsilon(m) =& 1 - \Lambda(m) \\ =& \frac{2}{\pi}\left[\arcsin\left(\frac{m}{2}\right) + \frac{m}{2}\sqrt{1 - \left(\frac{m}{2}\right)^2}\right], \quad |m| \le 2 \end{aligned} \tag{40}$$

but we do not do this in this paper.

For a single quadrant source, the TCC, for line structures varying in the direction along the axis of symmetry of the quadrant, is given Appendix A.3 and is shown in Figure 10a.

The even TCC after adding the two opposite quadrants is given in Appendix A.4 and is shown in Figure 10b. Unlike the case of semicircular condenser pupils, the TCC is not the same as that for a full circular condenser pupil. In particular, the mid-frequencies are enhanced.

The odd TCC after subtraction of two opposite quadrants is given in Appendix A.5 and is shown in Figure 10c.

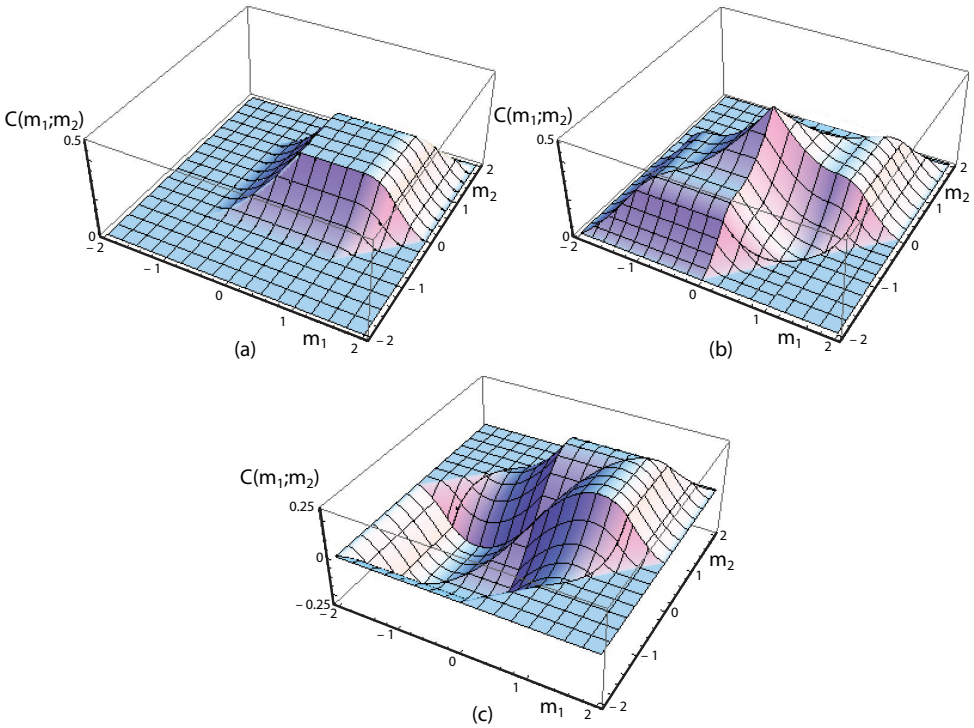

Figure 10. (**a**) The TCC ($C(m_1; m_2)$) for line structures for a system with a single-quadrant condenser pupil and a semicircular objective. (**b**) The TCC for AC, produced by adding the signals from two oppositely oriented quadrant pupils. This is twice the even component of (**a**). (**c**) The TCC for DPC, produced by subtracting the signals from two oppositely oriented quadrant pupils, equal to twice the odd component of (**a**).

11.2.2. First-Moment Condenser Pupil

For a first-moment condenser pupil, the TCC is given in Appendix A.5.1, as shown in Figure 11.

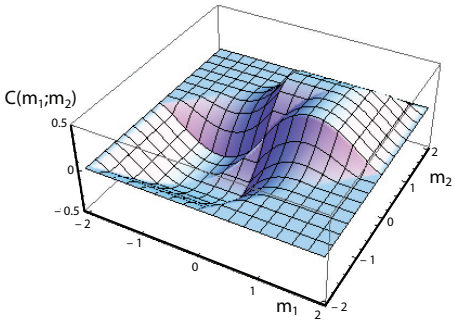

Figure 11. The TCC ($C(m_1; m_2)$) for line structures for a system with a first-moment condenser pupil and a circular objective.

11.2.3. Annular Condenser Pupil

For a slowly varying object, the image brightness depends on the variation in the PGTF with phase gradient. It has been shown that contrast can be greatly increased by using annular semicircular condenser pupils (equivalent to an annular detector in a scanning system) [32,33,35].

In Figure 8c, we show the TCC for a system with a thin annular semicircular condenser pupil where the inner radius of the annulus is equal to the radius of the objective pupil and the normalised thickness of the annulus is small. This behaves as a dark-field system, so weak objects are not imaged efficiently. The TCC can be separated into its DPC and AC components (odd and even in m, respectively), as shown in Figure 8a,d. DPC and AC

images can be formed by subtracting or adding the signals from two oppositely oriented annular semicircular sources. The PGTF is seen to rapidly increase in value from zero to 1 as m changes from 0 to the value of the annular normalised thickness, giving enhanced contrast for phase gradients in this range.

11.3. Semicircular Condenser Pupil with Semicircular Objective Pupil

11.3.1. Specular Case

In a reflection system, a specular microscope is a system with a semicircular condenser and a semicircular objective that accepts specular reflection from a level reflector, as in the slit lamp of ophthalmology [54]. The TCC for line structures is

$$\begin{aligned} C(m_1;m_2) &= \Lambda(2m_1), && |m_1| \geq |m_2|, \operatorname{sgn} m_2 = \operatorname{sgn} m_1 \\ &= \Lambda(2m_2), && |m_2| \geq |m_1|, \operatorname{sgn} m_2 = \operatorname{sgn} m_1 \\ &= \Lambda[2(m_1 - m_2)], && \operatorname{sgn} m_2 = -\operatorname{sgn} m_1, \end{aligned} \tag{41}$$

as shown in Figure 12a. The TCC is the same shape in this direction as for circular pupils but reduced in size by a factor of two because of the reduced semicircular width. The same result is achieved in transmission for a bright-field system with a semicircular condenser and a semicircular objective.

11.3.2. Dark-Field Case

For a dark-field system consisting of a semicircular objective pupil and a semicircular effective source, the TCC in the direction of the narrow cross-section for line structures is given in Appendix A.5.2 and is shown in Figure 12b. As the TCC is nonzero only in the first quadrant, the AC and DPC components in the first quadrant are just divided by two and repeated with positive or negative sign, respectively, in the third quadrant. Thus the AC and DPC components of a single measured image can be determined, in a similar way to single sideband (SSB) in radio communications, or to off-axis holography. Similarly (but without the division by two), if the signals from two oppositely oriented arrangements each with two semicircles, for the objective and condenser, are added, AC results, and if they are subtracted, DPC is obtained. These are shown in Figure 12c,d, respectively.

In these cases, the maximum spatial frequency in the image, given by the width of the nonzero region in the direction of $(m_1 - m_2) = m'$, is only half that for the system with a full circular objective pupil.

Smith and, independently, de Lang and Dekkers proposed a system with both condenser and objective pupils split into two semicircles, where the amplitudes could be adjusted using polarisation elements [55,56]. Ellis proposed, for visual observation, the use of a semicircular condenser pupil and an objective pupil with two semicircular regions of different strengths (say, 1 and a) [57]. If the amplitude of either objective semicircle is zero, then this reduces to either the specular (with $C_{SemiC/SemiO;Sp}$) or dark-field case (with $C_{SemiC/SemiO;DF}$), depending on the geometry. If $a = 1$, it reduces to a system with a semicircular condenser and a circular objective (with $C_{SemiC/CircO}$), as in Section 11.2. For the general case, it should be noted that the TCC is bilinear in P_O (Equation (2)) so that there is a cross-component, and the TCC is

$$C_a = C_{SemiC/SemiO;Sp} + a^2 C_{SemiC/SemiO;DF} + 2\Re(aC_{SemiC/SemiO;Cross}). \tag{42}$$

The cross-component is given by

$$2\Re(C_{SemiC/SemiO;Cross}) = C_{SemiC/CircO} - C_{SemiC/SemiO;Sp} - C_{SemiC/SemiO;DF} \tag{43}$$

so that, for real values of a,

$$C_a = aC_{SemiC/CircO} - a(1-a)C_{SemiC/SemiO;Sp} + (1-a)C_{SemiC/SemiO;DF}. \quad (44)$$

Note that the middle, specular term ($C_{SemiC/SemiO;Sp}$) vanishes if $a = 0$ or $a = 1$. In addition, we also have the connection with a DPC system with two semicircular condenser pupils:

$$C_{SemiC/CircO} = \frac{1}{2}(C_{CircC/CircO;AC} + C_{2\times SemiC/CircO;DPC}). \quad (45)$$

The TCC for the cross-component ($2C_{SemiC/SemiO;Cross}$), for the in-focus case, is given in Appendix A.5.3 and is shown in Figure 12e. It consists of two lobes, with the PGTF zero but not the WOTF.

11.4. Differential Interference Contrast

The TCC or PSI-window for DIC was given in Equation (9), which must also be multiplied by the TCC for a conventional microscope. It consists of three components with DPC, AC and DC symmetries, respectively. The total TCC can be separated into these three components. Phase-shifting DIC has been implemented by applying phase-shifting techniques to DIC images using the WOTF or PGTF approaches [36–38], but to the best of our knowledge, the separation of the complete TCC for partially coherent imaging has not been considered. In Figure 13, we show the TCC for line structures for a DIC microscope with an equal objective and condenser ($S = 1$) for the case when $\Delta = \pi/8$ and $\psi = \pi/4$. The total TCC is positive within its pass band. The PGTF ($m_2 = m_1$), showing the signal from a constant phase gradient, is asymmetric and responsible for the relief appearance of DIC images. Note that the intensity for weak positive slopes is almost level but falls off quickly for negative slopes (shadow casting). A larger value of $\Delta = \pi/4$ results in a small increase in intensity for positive slopes, giving a stronger highlighting appearance in Figure 14. However, this is accompanied by a zero in the PGTF and negative regions in the TCC within the pass band caused by the stronger DPC and DC components in this case. The DPC component is an odd function of m. Unlike the case of a semicircular condenser pupil, as in Figure 1d, the values of the WOTF ($m_2 = 0$) and the PGTF ($m_2 = m_1$) are different from each other for DIC. The AC component has a TCC that is very similar to that for a bright-field system as in Figure 1a, although the value for $m_2 = -m_1$ falls off slightly faster, resulting in poorer resolution for the AC component in the DIC case. The normalised DC component is weak compared with the other terms, and the weighted component is equal to zero for $\psi = \pi/4$, as shown in Figures 13a and 14a. For small values of ϕ, e.g., $\pi/10$, the DC component can become significant, resulting in significant nonlinear phase imaging in the total image for larger values of Δ (say, $\pi/10$).

To perform phase-stepping DIC, we take images with, for example, four values of ψ, with PSI-windows as follows:

$$\begin{aligned}
C'_0 &= \frac{1}{2}(\cos m'\Delta - \cos 2m\Delta)C'(m;m') = \sin m_1\Delta \sin m_2\Delta,\\
C'_{\pi/4} &= \frac{1}{2}(\cos 2m\Delta + \sin 2m\Delta)C'(m;m'),\\
C'_{\pi/2} &= \frac{1}{2}(\cos m'\Delta + \cos 2m\Delta)C'(m;m') = \cos m_1\Delta \cos m_2\Delta,\\
C'_{3\pi/4} &= \frac{1}{2}(\cos 2m\Delta - \sin 2m\Delta)C'(m;m'). \quad (46)
\end{aligned}$$

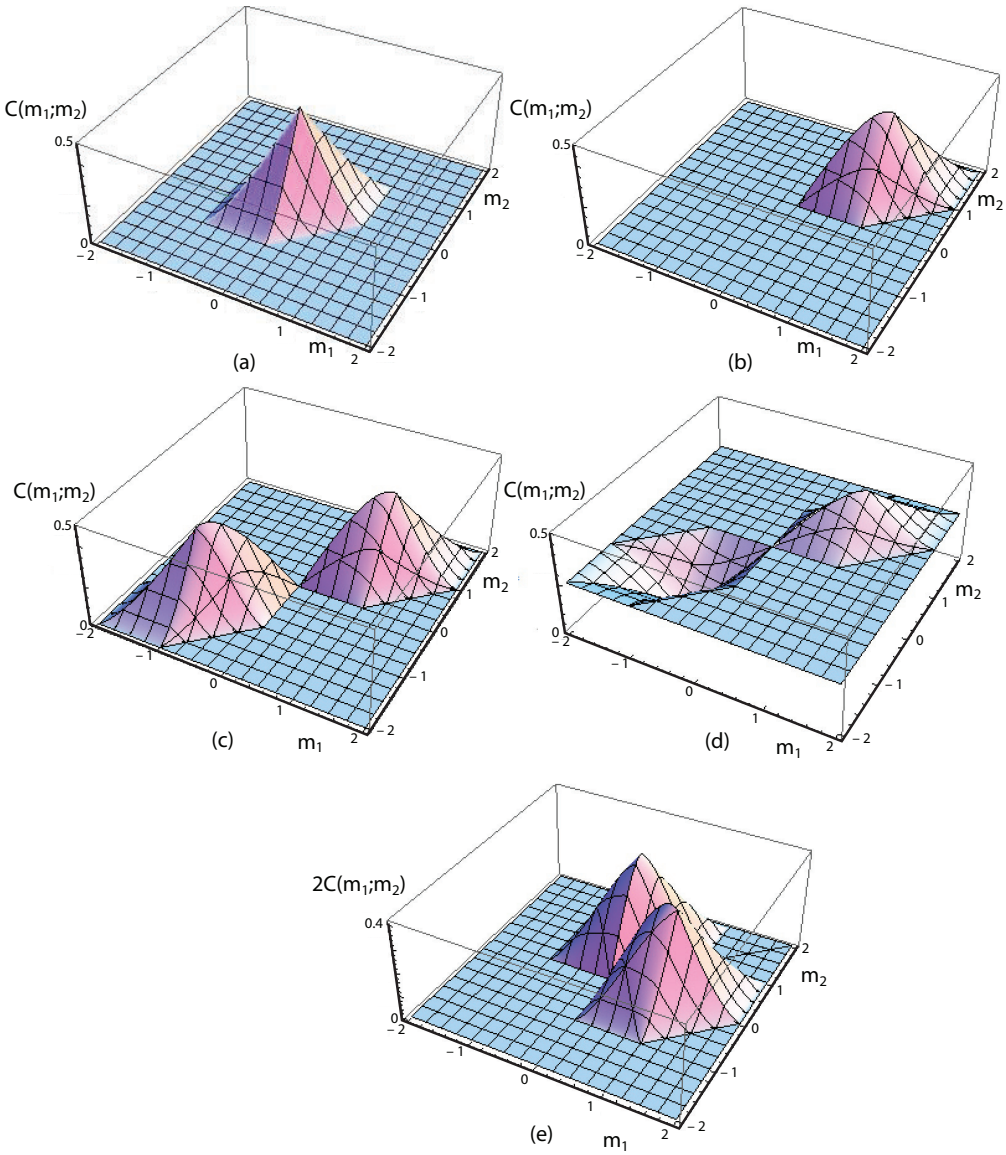

Figure 12. (**a**) The TCC ($C(m_1;m_2)$) for line structures for a system with a semicircular condenser pupil and a semicircular objective that accepts specular reflection from a level reflector, giving a specular microscope. (**b**) The TCC for a dark-field system consisting of a semicircular pupil and a semicircular effective source. (**c**) The AC TCC produced by adding the signals from two oppositely oriented semicircular pairs, equal to twice the even component of (**b**). (**d**) The TCC for DPC, produced by subtracting the signals from two oppositely oriented semicircular pairs, equal to twice the odd component of (**b**). (**e**) The cross-component for two semicircular objective pupil components.

The DC component is given by C'_0, the AC component by $C'_{\pi/2}$, and the DPC component by $(C'_{\pi/4} - C'_{3\pi/4}) = (2C'_{\pi/4} - C'_0 - C'_{\pi/2})/2 = \sin(2m\Delta)C'(m;m')$, where it is seen that only three measurements are actually necessary. The DPC component images the phase differential of weak phase objects. The premultiplier of $C'_{\pi/2} - C'_0 = \cos(2m\Delta)C'(m;m')$ is also independent of m'. For a slowly varying phase gradient, an image of the local phase derivative, proportional to $m(v)$, can then be obtained from $\arctan(I_{\pi/4} - I_{3\pi/4})/(I_{\pi/2} - I_0)/2\Delta$, the terms in m' and $C'(m;m')$, and the dependence on the object intensity transmittance (a^2), having all been cancelled. A conventional AC image can also be derived from $[(C'_{\pi/4} - C'_{3\pi/4})^2 + (C'_{\pi/2} - C'_0)^2]^{1/2}$.

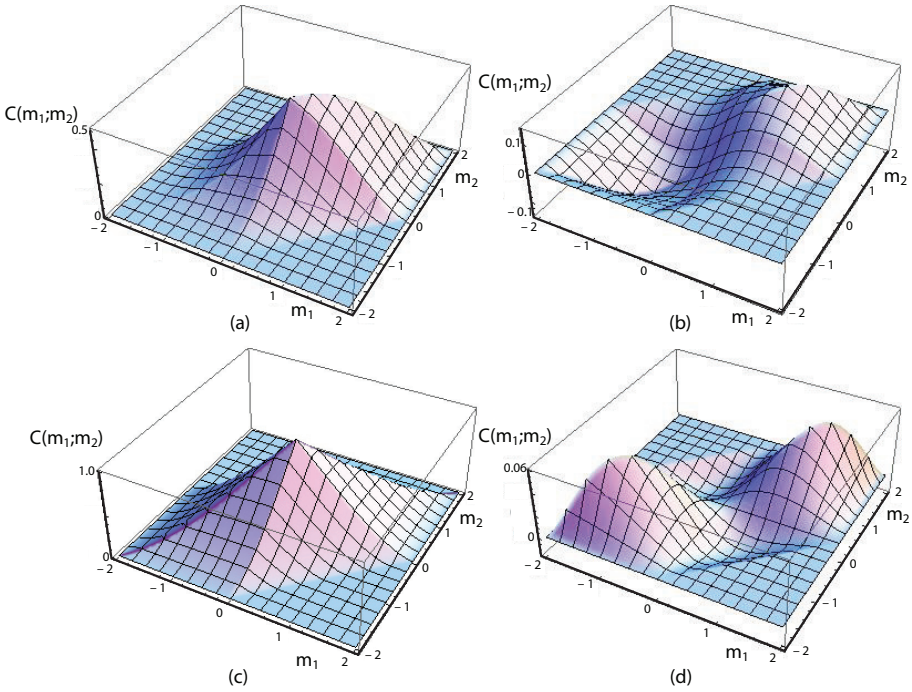

Figure 13. The TCC ($C(m_1; m_2)$) for line structures for a DIC system with $\Delta = \pi/8$ and $S = 1$. (**a**) The total TCC for $\psi = \pi/4$. (**b**) The normalised DPC component (without the $\sin 2\psi$ factor). (**c**) The normalised AC component (without the $\sin^2 \psi$ factor). (**d**) The normalised DC component (without the $\cos^2 \psi$ factor). The total TCC is given by the weighted sum of the three components.

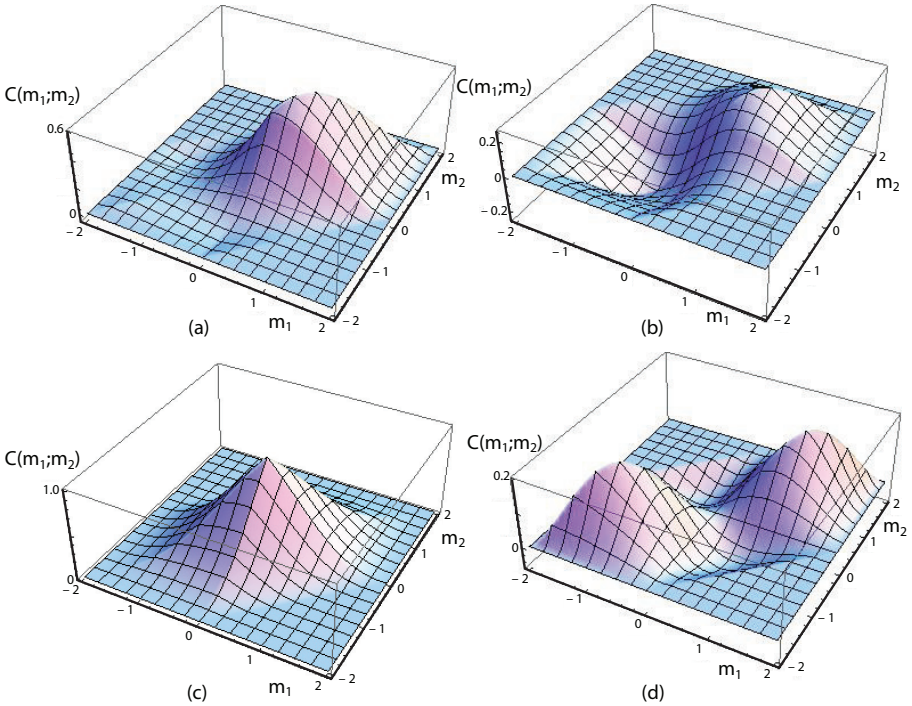

Figure 14. The TCC ($C(m_1; m_2)$) for line structures for a DIC system with $\Delta = \pi/4$ and $S = 1$. (**a**) The total TCC for $\psi = \pi/4$. (**b**) The normalised DPC component (without the $\sin 2\psi$ factor). (**c**): The normalised AC component (without the $\sin^2 \psi$ factor). (**d**): The normalised DC component (without the $\cos^2 \psi$ factor). The total TCC is given by the weighted sum of the three components.

12. Discussion

Plots of image intensity for coherent illumination of a phase grating have been presented. The results for a bright-field system are complicated and depend on the object

spatial frequency and the illumination offset. Images containing second or fourth harmonics of the object spatial frequency can be obtained. To obtain accurate results, inclusion of spatial frequencies up to the fourth harmonic is necessary in some cases.

We have discussed a few different ways of achieving phase contrast. The PGTFs ($C(m;m)$) for line structures for different cases are shown in Figure 15. These curves, which show the change in signal as the phase gradient is varied, are relevant for direct visual observation.

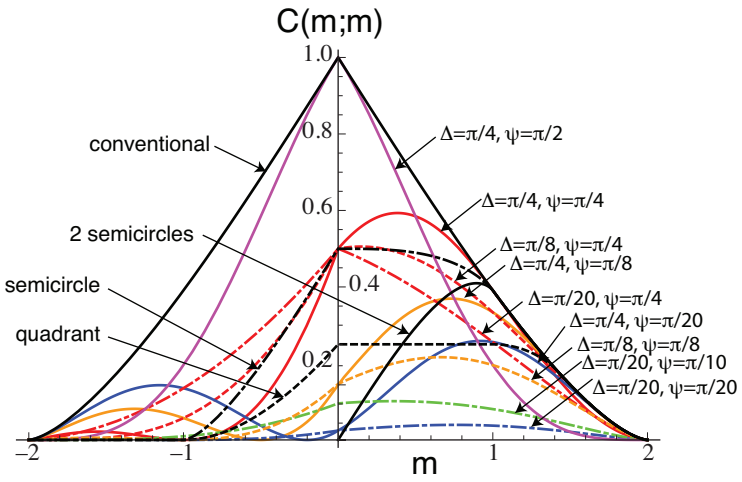

Figure 15. The total unnormalised PGTF ($C(m;m)$) for line structures for different optical systems, including DIC for particular parameters. Coloured solid lines refer to $\Delta = \pi/4$, dashed lines to $\Delta = \pi/8$, and chained lines to $\Delta = \pi/20$. Magenta lines refer to $\psi = \pi/2$, red lines to $\psi = \pi/4$, orange to $\psi = \pi/8$, and green to $\psi = \pi/10$. Curves are also shown (in black) for a conventional bright-field system (also obtained for $\psi = \pi/2$ and small Δ), a semicircular source, a quadrant source, and a semicircular source with a semicircular objective pupil (in the dark-field arrangement).

Curves of the total PGTF are given for DIC for various different values of the Δ and ψ parameters. The value of the bias (2ψ) fixes the value at the origin, ($m = 0$), as well as the strength of the DPC component, as given by the odd part of the curves. For a fixed value of bias, increasing Δ increases the strength of the cast shadow and highlighting effects. The are no zeros in the pass band for $\psi \geq 2\Delta$.

For comparison, we also show curves for some other microscope systems: a conventional bright-field system, a system with a single semicircular source, a single-quadrant source, and two semicircular pupils for the source and objective. In order to allow for easier comparison of the shapes of these curves, in Figure 16, we show some of the results after normalisation to $C(0;0) = 1$.

After digital processing, the DPC components can be extracted, the PGTF ($C_{DPC}(m;m)$) being an odd function of m, so now, $C(0;0) = 0$ and cannot be used to normalise the curves. Various cases are shown in Figure 17a. All the curves are calculated proportionally to the area of the source, except that the curve for annular semicircles (with a normalised thickness of 0.1 so that cut-off is at $m = 2.1$) has been multiplied by 5. This was calculated using the expressions for the convolution of two unequal circles given by Gaskill [58]. Note that the previous plots for an annular source have assumed a delta function annulus (Figure 8). For DIC, the PGTF for the DPC component is a function of Δ, but the shape is independent of ψ, with the curves shown being divided by the $\sin 2\psi$ factor. All the curves are odd and decay to zero at cut-off. Hence, two different values of the phase gradient correspond to a particular signal. At the maximum of $C_{DPC}(m;m)$, the signal is independent of changes in the phase gradient. For small values of the phase gradient, the signal is linearly related to the phase gradient.

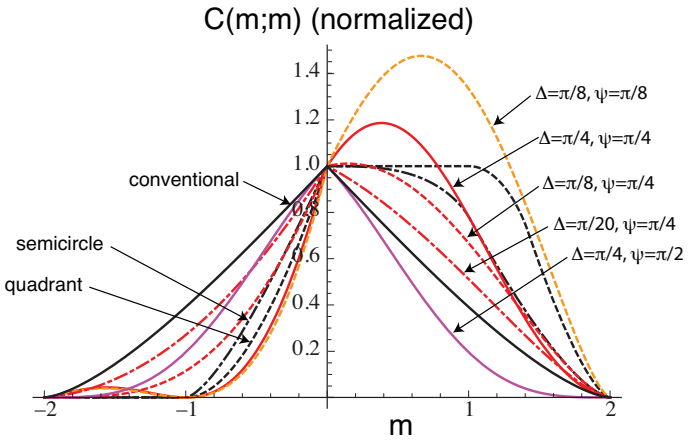

Figure 16. The total PGTF ($C(m;m)$) for line structures for different optical systems normalised to unity at $m = 0$, including DIC for particular parameters. Coloured solid lines refer to $\Delta = \pi/4$, dashed lines to $\Delta = \pi/8$, and chained lines to $\Delta = \pi/20$. Magenta lines refer to $\psi = \pi/2$, red lines to $\psi = \pi/4$, and orange to $\psi = \pi/8$. Curves are also shown (in black) for a conventional bright-field system (also obtained for $\psi = \pi/2$ and small Δ), a semicircular source, a quadrant source, and a semicircular source with a semicircular objective pupil (in the dark-field arrangement).

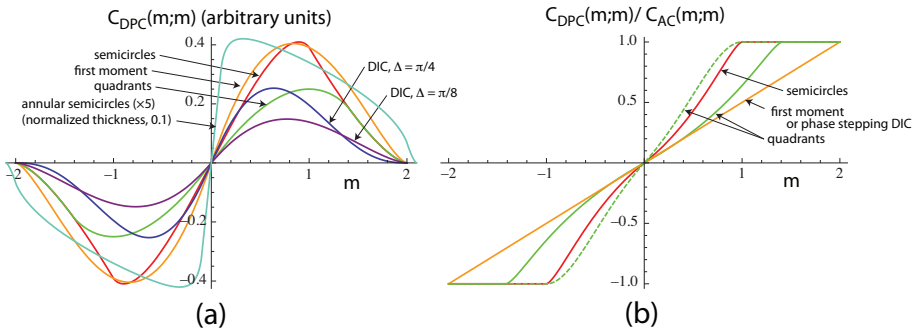

Figure 17. (**a**): DPC components of the PGTF ($C_{DPC}(m;m)$) for different systems: semicircular source (red line), a first-moment source (orange), annular semicircular source (cyan), quadrant source (green), DIC with $\Delta = \pi/4$ (blue), and DIC with $\Delta = \pi/8$ (purple). (**b**): The response to the phase gradient after normalising by the AC signal. For DIC, the AC component is the sum of $C_{AC}(m;m) + C_{DC}(m;m)$.

For DIC, after phase stepping, the measured phase gradient is linear up until cut-off (Figure 17b). For two semicircular condenser apertures, the signal after subtraction is proportional to $C_{DPC}(m;m)a^2 \mathrm{d}\phi/\mathrm{d}x$. After addition, the signal is $C_{AC}(m;m)a^2$, so dividing the DPC signal by the AC signal, the intensity transmittance a^2 cancels, and we obtain $[C_{DPC}(m;m)/C_{AC}(m;m)]\mathrm{d}\phi/\mathrm{d}x = [1 - \Lambda(2|m|)/\Lambda(|m|)]\mathrm{d}\phi/\mathrm{d}x$. The factor shown in square brackets is also plotted in Figure 17b. The response is reasonably linear up to $m = 1$. For quadrant detectors, the phase gradient can be measured in two orthogonal directions using either pairs of semicircles or pairs of quadrants. For pairs of quadrants, we have the choice of measuring the AC signal from the pairs of quadrants (dashed green line) or pairs of semicircles (solid green line), the former being reasonably linear up to $m = 1$ and the latter up to $m = \sqrt{2}$. For a first-moment source, and the response is linear right up to $m = 2$, but a separate measurement needs to be acquired for the AC component.

Author Contributions: Conceptualization, C.J.R.S., A.P.B. and M.R.; methodology, C.J.R.S., A.P.B. and M.R.; software, C.J.R.S.; validation, C.J.R.S., A.P.B. and M.R.; formal analysis, C.J.R.S.; investigation, C.J.R.S.; resources, M.R.; writing—original draft preparation, C.J.R.S.; writing—review and editing, A.P.B. and M.R.; visualization, C.J.R.S.; project administration, M.R. All authors have read and agreed to the published version of the manuscript.

Funding: This research received no external funding.

Institutional Review Board Statement: Not applicable.

Informed Consent Statement: Not applicable.

Data Availability Statement: The raw data supporting the conclusions of this article will be made available by the author upon request.

Conflicts of Interest: The authors declare no conflicts of interest.

Abbreviations

The following abbreviations are used in this manuscript:

AC	Amplitude contrast
ADF	Annular dark field
CDF	Central dark field
CTF	Coherent transfer function
DAC	Differential amplitude contrast
DC	Differential contrast
DIC	Differential interference contrast
DPC	Differential phase contrast
FM	Frequency modulation
iSCAT	Interference scattering
NA	Numerical aperture, $n \sin \alpha$
OTF	Optical transfer function
PC	Phase contrast
PGTF	Phase-gradient transfer function
PSI	Phase-space imager
SSB	Single sideband
TCC	Transmission cross-coefficient
WOTF	Weak object transfer function

Appendix A

The TCCs for different systems are given explicitly below.

Appendix A.1. Semicircular Condenser Pupil with Circular Objective Pupil

For a system with a semicircular condenser pupil and a circular objective pupil of equal radius, for line structures varying only in the direction of the narrow dimension of the semicircle, the TCC is

$$\begin{aligned} & C(m_1; m_2) \\ & = \Lambda(m_1) - \frac{1}{2}\Lambda(2m_1), && m_1 \geq m_2 \geq 0, \\ & = \Lambda(m_2) - \frac{1}{2}\Lambda(2m_2), && m_2 \geq m_1 \geq 0, \\ & = \Lambda(m_1 - m_2) - \frac{1}{2}\Lambda(2m_1), && 2 + m_2 \geq m_1 \geq -m_2 \geq 0, \\ & = \Lambda(m_2 - m_1) - \frac{1}{2}\Lambda(2m_2), && 2 + m_1 \geq m_2 \geq -m_1 \geq 0, \\ & = \frac{1}{2}\Lambda(2|m_2|) = 1 - \frac{1}{2}\Lambda(2m_2), && -m_2 \geq m_1 \geq m_2 \geq -1, \\ & = \frac{1}{2}\Lambda(2|m_1|) = 1 - \frac{1}{2}\Lambda(2m_1), && -m_1 \geq m_2 \geq m_1 \geq -1, \end{aligned} \tag{A1}$$

Appendix A.2. DPC with Two Semicircular Condenser Pupils and a Circular Objective Pupil

The TCC for DPC with two semicircular sources and a circular objective pupil is

$$\begin{aligned}
C(m_1;m_2) =& \Lambda(m_1) - \Lambda(2m_1), && m_1 \geq m_2 \geq 0,\\
=& \Lambda(m_2) - \Lambda(2m_2), && m_2 \geq m_1 \geq 0,\\
=& \Lambda(m_1 - m_2) - \Lambda(2m_1), && m_1 \geq -m_2 \geq 0,\\
=& \Lambda(m_2 - m_1) - \Lambda(2m_2), && -m_2 \geq m_1 \geq 0,\\
=& -\Lambda(m_1 - m_2) + \Lambda(2m_1), && -m_1 \geq m_2 \geq 0,\\
=& -\Lambda(m_2 - m_1) + \Lambda(2m_2), && m_2 \geq -m_1 \geq 0,\\
=& -\Lambda(|m_2|) + \Lambda(2|m_2|)\\
=& \Lambda(m_2) - \Lambda(2m_2), && 0 \geq m_1 \geq m_2,\\
=& -\Lambda(|m_1|) + \Lambda(2|m_1|)\\
=& \Lambda(m_1) - \Lambda(2m_1), && 0 \geq m_2 \geq m_1. \qquad \text{(A2)}
\end{aligned}$$

Appendix A.3. Quadrant Condenser Pupil with Circular Objective Pupil

For a single-quadrant source, the TCC, for line structures varying in the direction along the axis of symmetry of the quadrant, is

$$\begin{aligned}
&C(m_1;m_2)\\
&= \Lambda(m_1), && 2 \geq m_1 \geq \sqrt{2}\,\&\, m_1 \geq m_2 \geq 0,\\
&= \Lambda(m_2), && 2 \geq m_2 \geq \sqrt{2}\,\&\, m_2 \geq m_1 \geq 0,\\
&= \Omega(m_1), && \sqrt{2} \geq m_1 \geq 1\,\&\, 1 \geq m_1 \geq m_2,\\
&= \Omega(m_2), && \sqrt{2} \geq m_1 \geq 1\,\&\, 1 \geq m_2 \geq m_1,\\
&= \Omega(m_1) + \Omega(m_2), && \left(\sqrt{2} \geq m_1 \geq 1\,\&\, 0 \geq m_2 \geq -\sqrt{2 - m_1^2}\right),\\
& && \vee \left(\sqrt{2} \geq m_2 \geq 1\,\&\, 0 \geq m_1 \geq -\sqrt{2 - m_1^2}\right),\\
&= \frac{1}{4}, && 1 \geq m_1 \geq 0\,\&\, 1 \geq m_2 \geq 0,\\
&= \Lambda(m_1 - m_2), && \left(\sqrt{2} \geq m_1 \geq 1\,\&\, -\sqrt{2 - m_1^2} \geq m_2 \geq m_1 - 2\right)\\
& && \vee \left(2 \geq m_1 \geq \sqrt{2}\,\&\, 0 \geq m_2 \geq m_1 - 2\right),\\
&= \Lambda(m_2 - m_1), && \left(\sqrt{2} \geq m_2 \geq 1\,\&\, -\sqrt{2 - m_2^2} \geq m_1 \geq m_2 - 2\right)\\
& && \vee \left(2 \geq m_2 \geq \sqrt{2}\,\&\, 0 \geq m_1 \geq m_2 - 2\right),\\
&= \frac{1}{4} + \Omega(m_1), && 0 \geq m_2 \geq -1\,\&\, 1 \geq m_1 \geq m_2,\\
&= \frac{1}{4} + \Omega(m_2), && 0 \geq m_1 \geq -1\,\&\, 1 \geq m_2 \geq m_1, \qquad \text{(A3)}
\end{aligned}$$

Appendix A.4. AC from Quadrant Condenser Pupils with a Circular Objective Pupil

The even TCC after adding the two opposite quadrants is

$$
\begin{aligned}
&C(m_1;m_2)\\
&= \Lambda(m_1), && 2 \geq m_1 \geq \sqrt{2}\,\&\, m_1 \geq m_2 \geq 0,\\
&= \Lambda(m_2), && 2 \geq m_2 \geq \sqrt{2}\,\&\, m_2 \geq m_1 \geq 0,\\
&= \Omega(m_1), && \sqrt{2} \geq m_1 \geq 1\,\&\, m_1 \geq m_2 \geq 1,\\
&= \Omega(m_2), && \sqrt{2} \geq m_2 \geq 1\,\&\, m_2 \geq m_1 \geq 1,\\
&= \Lambda(m_1 - m_2), && \left(\sqrt{2} \geq m_1 \geq 1\,\&\, -\sqrt{2 - m_1^2} \geq m_2 \geq m_1 - 2\right)\\
&&& \quad \vee \left(2 \geq m_1 \geq \sqrt{2}\,\&\, 0 \geq m_2 \geq m_1 - 2\right),\\
&= \Lambda(m_2 - m_1), && \left(\sqrt{2} \geq m_2 \geq 1\,\&\, -\sqrt{2 - m_2^2} \geq m_1 \geq m_2 - 2\right)\\
&&& \quad \vee \left(2 \geq m_2 \geq \sqrt{2}\,\&\, 0 \geq m_1 \geq m_2 - 2\right),\\
&= \Omega(m_1) + \Omega(m_2), && \sqrt{2} \geq m_1 \geq 1\,\&\, 0 \geq m_2 \geq -\sqrt{2 - m_1^2},\\
&= -[\Omega(m_1) + \Omega(m_2)], && \sqrt{2} \geq m_2 \geq 1\,\&\, 0 \geq m_1 \geq -\sqrt{2 - m_2^2},\\
&= \frac{1}{2} - \Omega(m_1), && 1 \geq m_1 \geq 0\,\&\, m_1 \geq m_2 \geq 0,\\
&= \frac{1}{2} + \Omega(m_1), && -1 \leq m_1 \leq 0\,\&\, m_2 \leq m_1 \leq 0,\\
&= \frac{1}{2} - \Omega(m_2), && 1 \geq m_2 \geq 0\,\&\, m_2 \geq m_1 \geq 0,\\
&= \frac{1}{2} + \Omega(m_2), && -1 \leq m_2 \leq 0\,\&\, m_1 \leq m_2 \leq 0,\\
&= \frac{1}{2} - \Omega(m_1) + \Omega(m_2), && 1 \geq m_1 \geq 0\,\&\, 0 \geq m_2 \geq -1,\\
&= \frac{1}{2} + \Omega(m_1) - \Omega(m_2), && -1 \leq m_1 \leq 0\,\&\, 0 \leq m_2 \leq 1,\\
&= -[\Omega(m_1) + \Omega(m_2)], && -1 \geq m_2 \geq -\sqrt{2}\,\&\, \sqrt{2 - m_2^2} \geq m_1 \geq 0,\\
&= \Omega(m_1) + \Omega(m_2), && -1 \geq m_1 \geq -\sqrt{2}\,\&\, \sqrt{2 - m_1^2} \geq m_2 \geq 0,\\
&= \Lambda(m_1 - m_2), && \left(-\sqrt{2} \leq m_1 \leq -1\,\&\, \sqrt{2 - m_1^2} \leq m_2 \leq m_1 + 2\right)\\
&&& \quad \vee \left(2 \geq m_1 \geq \sqrt{2}\,\&\, 0 \geq m_2 \geq m_1 - 2\right),\\
&= \Lambda(m_2 - m_1), && \left(-\sqrt{2} \leq m_2 \leq -1\,\&\, \sqrt{2 - m_2^2} \leq m_1 \leq m_2 + 2\right)\\
&&& \quad \vee \left(2 \geq m_2 \geq \sqrt{2}\,\&\, 0 \geq m_1 \geq m_2 - 2\right),\\
&= -\Omega(m_1), && -\sqrt{2} \leq m_1 \leq -1\,\&\, m_1 \leq m_2 \leq 0,\\
&= -\Omega(m_2), && -\sqrt{2} \leq m_2 \leq -1\,\&\, m_2 \leq m_1 \leq 0,\\
&= \Lambda(|m_1|), && -2 \leq m_1 \leq -\sqrt{2}\,\&\, m_1 \leq m_2 \leq 0,\\
&= \Lambda(|m_2|), && -2 \leq m_2 \leq -\sqrt{2}\,\&\, m_2 \leq m_1 \leq 0,
\end{aligned}
\tag{A4}
$$

Appendix A.5. DPC from Quadrant Condenser Pupils with a Circular Objective Pupil

The odd TCC after subtraction of two opposite quadrants is

$$
\begin{aligned}
&C(m_1;m_2)\\
&\quad=\Lambda(m_1), && 2\geq m_1\geq\sqrt{2}\,\&\,m_1\geq m_2\geq 0,\\
&\quad=\Lambda(m_2), && 2\geq m_2\geq\sqrt{2}\,\&\,m_2\geq m_1\geq 0,\\
&\quad=\Omega(m_1), && \sqrt{2}\geq m_1\geq 1\,\&\,m_1\geq m_2\geq 0,\\
&\quad=\Omega(m_2), && \sqrt{2}\geq m_2\geq 1\,\&\,m_2\geq m_1\geq 0,\\
&\quad=\Lambda(m_1-m_2), && \left(\sqrt{2}\geq m_1\geq 1\,\&\,-\sqrt{2-m_1^2}\geq m_2\geq m_1-2\right)\\
&\qquad && \vee\left(2\geq m_1\geq\sqrt{2}\,\&\,0\geq m_2\geq m_1-2\right),\\
&\quad=\Lambda(m_2-m_1), && \left(\sqrt{2}\geq m_2\geq 1\,\&\,-\sqrt{2-m_2^2}\geq m_1\geq m_2-2\right)\\
&\qquad && \vee\left(2\geq m_2\geq\sqrt{2}\,\&\,0\geq m_1\geq m_2-2\right),\\
&\quad=\Omega(m_1)+\Omega(m_2), && \left(2\geq m_1\geq 0\,\&\,0\geq m_2\geq-\sqrt{2-m_1^2}\right),\\
&\qquad && \vee\left(-2\leq m_1\leq 0\,\&\,0\leq m_2\leq\sqrt{2-m_1^2}\right),\\
&\quad=-\Lambda(m_1-m_2), && \left(-\sqrt{2}\leq m_1\leq -1\,\&\,\sqrt{2-m_1^2}\leq m_2\leq m_1+2\right)\\
&\qquad && \vee\left(2\geq m_1\geq\sqrt{2}\,\&\,0\geq m_2\geq m_1-2\right),\\
&\quad=-\Lambda(m_2-m_1), && \left(-\sqrt{2}\leq m_2\leq -1\,\&\,\sqrt{2-m_2^2}\leq m_1\leq m_2+2\right)\\
&\qquad && \vee\left(2\geq m_2\geq\sqrt{2}\,\&\,0\geq m_1\geq m_2-2\right),\\
&\quad=\Omega(m_1), && -\sqrt{2}\leq m_1\leq -1\,\&\,m_1\leq m_2\leq 0,\\
&\quad=\Omega(m_2), && -\sqrt{2}\leq m_2\leq -1\,\&\,m_2\leq m_1\leq 0,\\
&\quad=-\Lambda(|m_1|), && -2\leq m_1\leq-\sqrt{2}\,\&\,m_1\leq m_2\leq 0,\\
&\quad=-\Lambda(|m_2|), && -2\leq m_2\leq-\sqrt{2}\,\&\,m_2\leq m_1\leq 0,
\end{aligned}
\tag{A5}
$$

Appendix A.5.1. First-Moment Condenser Pupil

For a first-moment condenser pupil, the TCC is

$$
\begin{aligned}
C(m_1;m_2)=&m_1\Lambda(|m_1|),\\
&(m_1\geq m_2\geq 0)\,\&\,(0\geq m_2\geq m_1),\\
=&m_2\Lambda(|m_2|),\\
&(m_2\geq m_1\geq 0)\,\&\,(0\geq m_1\geq m_2),\\
=&(m_1+m_2)\Lambda(|m_1-m_2|),\\
&(m_1\geq 0\geq m_2)\,\&\,(m_2\geq 0\geq m_1),
\end{aligned}
\tag{A6}
$$

Appendix A.5.2. Dark-Field Case of a Semicircular Source and a Semicircular Objective Pupil

For a dark-field system consisting of a semicircular effective source and a semicircular objective pupil, the TCC, in the direction of the narrow cross-section, for line structures is

$$
\begin{aligned}
C(m_1;m_2) =& \Lambda(m_1) - \frac{1}{2}\Lambda(2m_1) - \frac{1}{2}\Lambda(2m_2), \\
& 4 \geq 2m_1 \geq 2m_2 \geq m_1 > 0, \\
=& \Lambda(m_2) - \frac{1}{2}\Lambda(2m_2) - \frac{1}{2}\Lambda(2m_1), \\
& 4 \geq 2m_2 \geq 2m_1 \geq m_2 > 0, \\
=& \frac{1}{2}\Lambda[2(m_1 - m_2)] - \frac{1}{2}\Lambda(2m_1), \\
& 2 \geq m_1 \geq 2m_2 > 0, \\
=& \frac{1}{2}\Lambda[2(m_1 - m_2)] - \frac{1}{2}\Lambda(2m_2), \\
& 2 \geq m_2 \geq 2m_1 > 0,
\end{aligned} \tag{A7}
$$

Appendix A.5.3. The Cross-Component for Two Semicircular Sources and a Semicircular Objective Pupil

The TCC for the cross-component ($2C_{SemiC/SemiO;Cross}$) for the in-focus case is

$$
\begin{aligned}
2C(m_1;m_2) =& \Lambda(m_1) - \frac{1}{2}\Lambda(2m_1), && 1 \geq m_1 \geq 2m_2 \geq 0, \\
=& \Lambda(m_2) - \frac{1}{2}\Lambda(2m_2), && 1 \geq m_2 \geq 2m_1 \geq 0, \\
=& \frac{1}{2}\Lambda(2m_2) - \frac{1}{2}\Lambda(2m_1), && 1 \geq m_1 \geq 2m_2 \geq 2m_1 \geq 0, \\
=& \frac{1}{2}\Lambda(2m_1) - \frac{1}{2}\Lambda(2m_2), && 1 \geq m_2 \geq 2m_1 \geq 2m_2 \geq 0, \\
=& \Lambda(m_1 - m_2) - \frac{1}{2}\Lambda(2m_1) - \frac{1}{2}\Lambda[2(m_1 - m_2)], && 2 \geq m_1 \geq -m_2 \geq 0, \\
=& \Lambda(m_2 - m_1) - \frac{1}{2}\Lambda(2m_2) - \frac{1}{2}\Lambda[2(m_2 - m_1)], && 2 \geq m_2 \geq -m_1 \geq 0, \\
=& \frac{1}{2}\Lambda(2|m_2|) - \frac{1}{2}\Lambda[2(m_1 - m_2)], && 1 \geq -m_2 \geq m_1 \geq 0, \\
=& \frac{1}{2}\Lambda(2|m_1|) - \frac{1}{2}\Lambda[2(m_2 - m_1)], && 1 \geq -m_1 \geq m_2 \geq 0,
\end{aligned} \tag{A8}
$$

References

1. Blood, A.P.; Sheppard, C.J.R.; Roy, M. Dual-illumination Fourier modulation microscopy: New techniques for multimodal light imaging. *Microsc. Res. Tech.* **2026**, *89*, 769–783. [CrossRef]
2. Abbe, E.; Fripp, H. A contribution to the theory of the microscope, and the nature of microscopic vision (English translation). *Proc. Bristol Nat. Soc. New Ser.* **1874**, *1*, 200–258.
3. Köhler, H. On Abbe's theory of image formation in the microscope. *Opt. Acta* **1981**, *28*, 1691–1701. [CrossRef]
4. Rayleigh, J.W.S. On the theory of optical images, with special reference to the microscope. *Philos. Mag.* **1896**, *42*, 167–195. [CrossRef]
5. Rayleigh, J.W.S. VIII—On the theory of optical images, with special reference to the microscope (Supplementary paper). *J. R. Microsc. Soc.* **1903**, *23*, 474–482. [CrossRef]
6. Hopkins, H. On the diffraction theory of optical images. *Proc. R. Soc. Lond. Ser. A* **1953**, *217*, 408–432. [CrossRef]
7. Saleh, B.E.A.; Rabbani, M. Simulation of partially coherent imagery in the space and frequency domains and by modal expansion. *Appl. Opt.* **1982**, *21*, 2770–2777. [CrossRef]
8. Yamazoe, K. Two models for partially coherent imaging. *J. Opt. Soc. Am. A* **2012**, *29*, 2591–2597. [CrossRef]
9. Burge, R.E.; Dainty, J.C. Partially coherent image formation in the scanning transmission electron microscope. *Optik* **1976**, *46*, 229–240.
10. Burge, R.E.; Browne, M.T.; Charalambous, P.; Clark, A.; Wu, J.K. Multiple signals in STEM. *J. Microsc.* **1982**, *127*, 47–60. [CrossRef] [PubMed]
11. Swing, R.; Clay, J. Ambiguity of the transfer function with partially coherent illumination. *J. Opt. Soc. Am.* **1967**, *57*, 1180–1189. [CrossRef]

12. Nyyssonen, D. Linewidth measurement with an optical microscope: The effect of operating conditions on the image profile. *Appl. Opt.* **1977**, *16*, 2223–2230. [CrossRef]
13. Kermisch, D. Partially coherent image processing by laser scanning. *J. Opt. Soc. Am.* **1975**, *65*, 887–891. [CrossRef]
14. Papoulis, A. Ambiguity function in Fourier optics. *J. Opt. Soc. Am.* **1974**, *64*, 779–788. [CrossRef]
15. Mehta, S.B.; Sheppard, C.J.R. Phase-space representation of partially-coherent imaging systems using the Cohen class distribution. *Opt. Lett.* **2010**, *35*, 348–350. [CrossRef]
16. Hopkins, H.H.; Barham, P.M. The influence of the condenser on microscopic resolution. *Proc. Phys. Soc.* **1950**, *63*, 737–744. [CrossRef]
17. Zernike, F. Phase contrast, a new method for the microscopic observation of transparent object. *Physica* **1942**, *9*, 686–693. 974–986.
18. Mehta, S.B.; Sheppard, C.J.R. An equivalent of the point spread function for partially coherent imaging. *Optica* **2015**, *2*, 736–739. [CrossRef]
19. McKechnie, T.S. The effect of condenser obstruction on the two point resolution of a microscope. *Opt. Acta* **1972**, *19*, 729–737. [CrossRef]
20. Watrasiewicz, B.M. Theoretical calculations of images of straight edges in partially coherent illumination. *Opt. Acta* **1965**, *12*, 391–400. [CrossRef]
21. Kinzly, R.E. Investigations of the influence of the degree of coherence upon images of objects. *J. Opt. Soc. Am.* **1965**, *55*, 1002–1007. [CrossRef]
22. Kinzly, R.E. Images of coherently illuminated edged objects formed by scanning optical systems. *J. Opt. Soc. Am.* **1966**, *56*, 9–11. [CrossRef]
23. Yamamoto, K.; Ichioka, Y.; Suzuki, T. Influence of light coherence at the exit pupil of the condenser on the image formation. *Opt. Acta* **1976**, *23*, 987–996. [CrossRef]
24. Welford, W.T. On the relationship between the modes of image formation in scanning microscopy and conventional microscopy. *J. Microsc.* **1972**, *96*, 105. [CrossRef]
25. Sheppard, C.J.R.; Choudhury, A. Image formation in the scanning microscope. *Opt. Acta* **1977**, *24*, 1051–1073. [CrossRef]
26. Sheppard, C.J.R.; Wilson, T. Image formation in scanning microscopes with partially coherent source and detector. *Opt. Acta* **1978**, *25*, 315–325. [CrossRef]
27. Sheppard, C.J.R.; Wilson, T. The theory of the direct-view confocal microscope. *J. Microsc.* **1981**, *124*, 107–117. [CrossRef]
28. Kintner, E.C. Method for the calculation of partially coherent imagery. *Appl. Opt.* **1978**, *17*, 2747–2753. [CrossRef] [PubMed]
29. Möller, B.O. Imaging of a straight edge in partially coherent illumination in the presence of spherical aberrations. *Opt. Acta* **1968**, *15*, 223–236. [CrossRef]
30. Mehta, S.B.; Sheppard, C.J.R. Quantitative phase-gradient imaging at high resolution with asymmetric illumination-based differential phase contrast. *Opt. Lett.* **2009**, *34*, 1924–1926. [CrossRef]
31. Dekkers, N.H.; de Lang, H. Differential phase contrast in a STEM. *Optik* **1974**, *41*, 452–456.
32. Rose, H. Nonstandard imaging methods in electron microscopy. *Ultramicroscopy* **1977**, *2*, 251–267. [CrossRef] [PubMed]
33. Morrison, G.R.; Chapman, J.N. A comparison of three differential phase contrast systems suitable for use in STEM. *Optik* **1983**, *64*, 1–12.
34. Hamilton, D.K.; Sheppard, C.J.R. Differential phase contrast in scanning optical microscopy. *J. Microsc.* **1984**, *133*, 27–39. [CrossRef]
35. Hamilton, D.K.; Sheppard, C.J.R.; Wilson, T. Improved imaging of phase gradients in scanning optical microscopy. *J. Microsc.* **1984**, *135*, 275–286. [CrossRef]
36. Ishiwata, H.; Itoh, M.; Yatagai, T. Retardation modulated differential interference microscope and its application to 3-D shape measurement. *Proc. SPIE* **1996**, *2873*, 21–24.
37. Cogswell, C.J.; Smith, N.I.; Larkin, K.G.; Hariharan, P. Quantitative DIC microscopy using a geometric phase shifter. *Proc. SPIE* **1997**, *2984*, 72–81.
38. Ishiwata, H.; Itoh, M.; Yatagai, T. A new method of three-dimensional measurement by differential interference contrast microscope. *Opt. Commun.* **2006**, *260*, 117–126. [CrossRef]
39. Arnison, M.R.; Larkin, K.G.; Sheppard, C.J.R.; Smith, N.I.; Cogswell, C.J. Linear phase imaging using differential interference microscopy. *J. Microsc.* **2004**, *214*, 7–12. [CrossRef]
40. Streibl, N. Phase imaging by the transport equation of intensity. *Opt. Commun.* **1984**, *49*, 6–10. [CrossRef]
41. Paganin, D.; Nugent, K.A. Noninterferometric phase imaging with partially coherent light. *Phys. Rev. Lett.* **1998**, *80*, 2586–2589. [CrossRef]
42. Kou, S.S.; Waller, L.; Barbastathis, G.; Marquet, P.; Depeursinge, C.; Sheppard, C.J.R. Quantitative phase restoration by direct inversion using the optical transfer function. *Opt. Lett.* **2011**, *36*, 2671–2673. [CrossRef]

43. Mehta, S.B.; Sheppard, C.J.R. Using the phase-space imager to analyze partially coherent imaging systems: Bright-field, phase contrast, differential interference contrast, differential phase contrast, and spiral phase contrast. *J. Mod. Opt.* **2010**, *57*, 718–739. [CrossRef]
44. Wilson, T.; Sheppard, C.J.R. Coded apertures and detectors for optical differentiation. *Proc. SPIE* **1980**, *232*, 203–209.
45. Cogswell, C.J.; Sheppard, C.J.R. Confocal differential interference contrast (DIC) microscopy: Including a theoretical analysis of conventional and confocal (DIC) imaging. *J. Microsc.* **1992**, *165*, 81–101. [CrossRef]
46. Sheppard, C.J.R.; Wilson, T. Fourier imaging of phase information in conventional and scanning microscopes. *Philos. Trans. R. Soc. Lond.* **1980**, *295*, 513–536. [CrossRef]
47. Mehta, S.B.; Sheppard, C.J.R. Partially coherent image formation in differential interference contrast (DIC) microscope. *Opt. Express* **2008**, *16*, 19462–19469. [CrossRef] [PubMed]
48. Allen, R.D.; Allen, N.S.; Travis, J.L. Video-enhanced contrast, differential interference contrast (AVEC-DIC) microscopy: A new method capable of analysing microtubule related mobility in the reticulopodial network of allogromia laticollaris. *Cell Motil.* **1981**, *1*, 291–302. [CrossRef]
49. Allen, R.D.; Allen, N.S. Video-enhanced microscopy with a computer frame memory. *J. Microsc.* **1983**, *129*, 3–17. [CrossRef]
50. Oliver, B.M. Signal-to-noise ratios in photoelectric mixing. *Proc. IRE* **1961**, *49*, 1960–1961.
51. Kukura, P.; Ewers, H.; Müller, C.; Renn, A.; Helenius, A.; Sandoghdar, V. High-speed nanoscopic tracking of the position and orientation of a single virus. *Nat. Methods* **2009**, *6*, 923–927. [CrossRef]
52. Mondal, P.K.; S, S. Images de Bords de Phase en Eclairage Partiellement Cohérent en Microscopie à Contraste de Phase. *Opt. Acta* **1970**, *17*, 425–437. [CrossRef]
53. Gan, X.S.; Sheppard, C.J.R. Imaging in a confocal microscope with one circular and one annular lens. *Opt. Commun.* **1993**, *103*, 254–264. [CrossRef]
54. Maurice, D.M. Cellular membrane activity in the corneal endothelium of the intact eye. *Experientia* **1968**, *15*, 1094–1095. [CrossRef]
55. Smith, F.H. Improvements in or Relating to Microscopy. UK Patent No. 634,048, 1950.
56. de Lang, H.; Dekkers, N.H. Microscope adapted for the generation of various contrast types: Theory and experiment. *Appl. Opt.* **1977**, *16*, 2215–2222. [CrossRef]
57. Ellis, G.W. Edge Enhancement of Phase Phenomena. U.S. Patent No. 4,255,014, 1981.
58. Gaskill, J.D. *Linear Systems, Fourier Transforms, and Optics*; Wiley: New York, NY, USA, 1978.

Disclaimer/Publisher's Note: The statements, opinions and data contained in all publications are solely those of the individual author(s) and contributor(s) and not of MDPI and/or the editor(s). MDPI and/or the editor(s) disclaim responsibility for any injury to people or property resulting from any ideas, methods, instructions or products referred to in the content.